

Mechanics of Fold-and-Thrust Belts and Accretionary Wedges

DAN DAVIS

*Department of Earth and Planetary Sciences, Massachusetts Institute of Technology
Cambridge, Massachusetts 02139*

JOHN SUPPE AND F. A. DAHLEN

*Department of Geological and Geophysical Sciences, Guyot Hall, Princeton University
Princeton, New Jersey 08544*

The overall mechanics of fold-and-thrust belts and accretionary wedges along compressive plate boundaries is considered to be analogous to that of a wedge of soil or snow in front of a moving bulldozer. The material within the wedge deforms until a critical taper is attained, after which it slides stably, continuing to grow at constant taper as additional material is encountered at the toe. The critical taper is the shape for which the wedge is on the verge of failure under horizontal compression everywhere, including the basal decollement. A wedge of less than critical taper will not slide when pushed but will deform internally, steepening its surface slope until the critical taper is attained. Common silicate sediments and rocks in the upper 10–15 km of the crust have pressure-dependent brittle compressive strengths which can be approximately represented by the empirical Coulomb failure criterion, modified to account for the weakening effects of pore fluid pressure. A simple analytical theory that predicts the critical tapers of subaerial and submarine Coulomb wedges is developed and tested quantitatively in three ways: First, laboratory model experiments with dry sand match the theory. Second, the known surface slope, basal dip, and pore fluid pressures in the active fold-and-thrust belt of western Taiwan are used to determine the effective coefficient of internal friction within the wedge, $\mu = 1.03$, consistent with Byerlee's empirical law of sliding friction, $\mu_b = 0.85$, on the base. This excess of internal strength over basal friction suggests that although the Taiwan wedge is highly deformed by imbricate thrusting, it is not so pervasively fractured that frictional sliding is always possible on surfaces of optimum orientation. Instead, the overall internal strength apparently is controlled by frictional sliding along suboptimally oriented planes and by the need to fracture some parts of the observed geometrically complex structure for continued deformation. Third, using the above values of μ_b and μ , we predict Hubbert-Rubey fluid pressure ratios $\lambda = \lambda_b$ for a number of other active subaerial and submarine accretionary wedges based on their observed tapers, finding values everywhere in excess of hydrostatic. These predicted overpressures are reasonable in light of petroleum drilling experience in general and agree with nearby fragmentary well data in specific wedges where they are available. The pressure-dependent Coulomb wedge theory developed here is expected to break down if the decollement exhibits pressure-independent plastic behavior because of either temperature or rock type. The effects of this breakdown are observed in the abrupt decrease in taper where wedge thicknesses exceed about 15 km, which is the predicted depth of the brittle-plastic transition in quartz-rich rocks for typical geothermal gradients. We conclude that fold-and-thrust belts and accretionary wedges have the mechanics of bulldozer wedges in compression and that normal laboratory fracture and frictional strengths are appropriate to mountain-building processes in the upper crust, above the brittle-plastic transition.

INTRODUCTION

The zones of folding and thrusting that lie along the margins of many mountain belts constitute one of the most widely recognized and best understood deformational features of the earth [McClay and Price, 1981]. Previous models and theories of the mechanics of fold-and-thrust belts have been based largely on observations of belts that are no longer tectonically active, simply because there has been more geological exploration of these inactive areas (for example, Figures 1a and 1b). Additional insight may be gained by examining the relatively few active fold-and-thrust belts, such as the Himalayan foothills and western Taiwan (Figure 1c). Furthermore, a great deal of geophysical information is now available for the oceanic analogue of fold-and-thrust belts, namely, the accretionary wedges in front of island arcs (for example, Beck and Lehner [1974], Seely et al. [1974], Hamilton [1979], and Nasu et al. [1979]). In this paper we

present a simple mechanical model of fold-and-thrust belts and accretionary wedges based on active examples, particularly western Taiwan.

Although considerable natural variation exists among the many fold-and-thrust belts and accretionary wedges of the earth, several common properties occur in cross section that might form the basis of a successful theory of their mechanics. Chapple [1978] emphasized that fold-and-thrust belts and accretionary wedges exhibit: (1) a basal surface of detachment or decollement, below which there is little deformation, dipping toward the interior of the mountain belt; (2) large horizontal compression in the material above the basal decollement; and (3) a characteristic wedge shape of the deformed material, tapering toward the margin of the mountain belt (see Figure 1). The overall mechanics of these wedges along compressive plate boundaries is considered by Chapple [1978], Davis and Suppe [1980], Stockmal and Chapple [1981], and others to be analogous to the mechanics of wedges that form in front of moving bulldozers or snow plows. Such bulldozer and snowplow wedges have the same three properties, but on a smaller scale. The soil, snow, or rock deforms until the wedge attains a steady state or critical

Copyright 1983 by the American Geophysical Union.

Paper number 2B1741.
0148-0227/83/002B-1741\$05.00

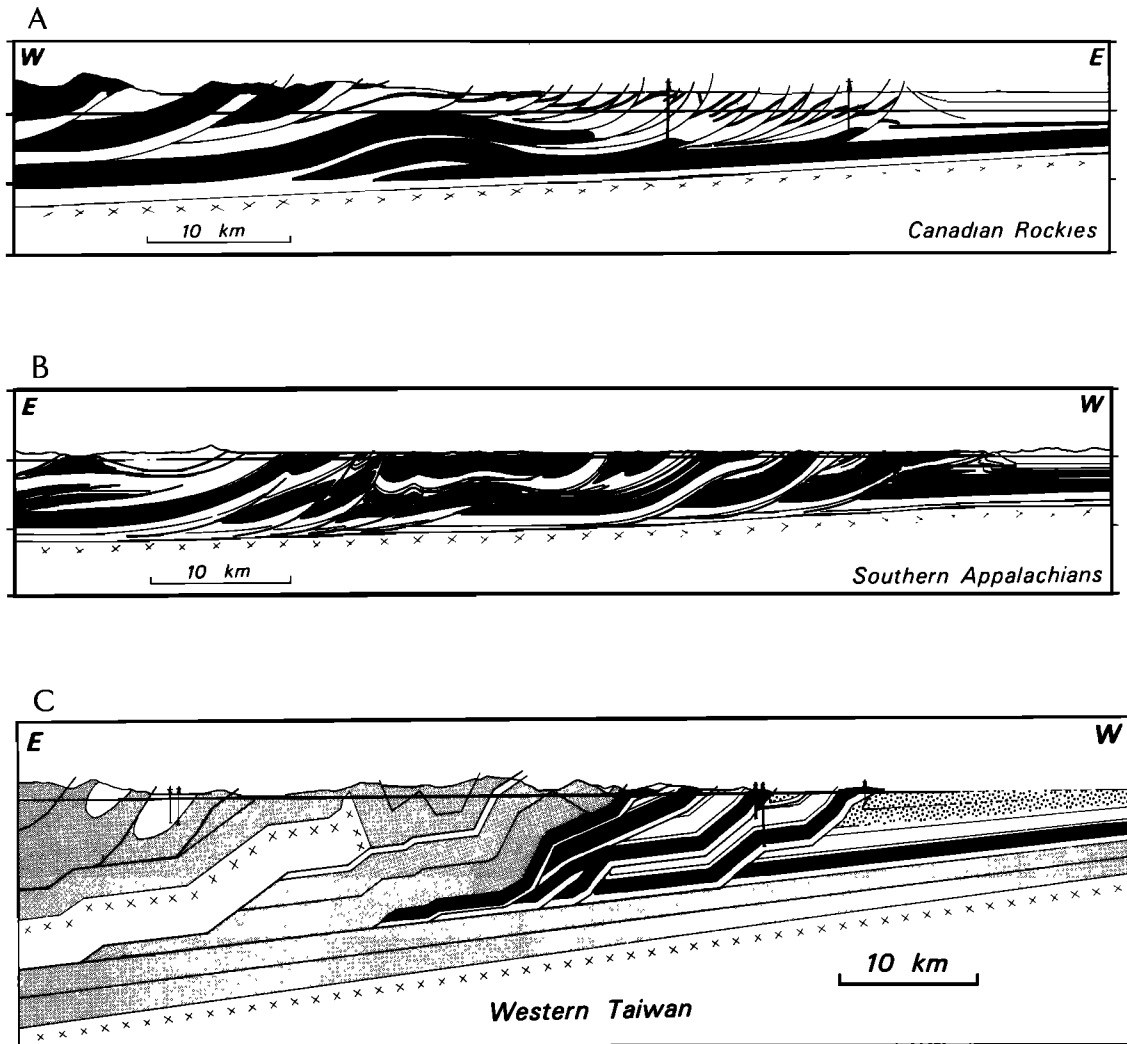


Fig. 1. Cross sections of several foreland fold-and-thrust belts: (a) Canadian Rockies [after Bally *et al.*, 1966], (b) southern Appalachians [after Roeder *et al.*, 1978], and (c) western Taiwan [after Suppe, 1980a].

taper and then slides stably, continuing to grow self-similarly as additional material is accreted at the toe. A critically tapered wedge that is not accreting fresh material is the thinnest body that can be thrust over its basal decollement without any internal deformation; it is thus on the verge of shear failure everywhere. In contrast, a critically tapered wedge that is accreting fresh material deforms internally while sliding in order to accommodate the influx and to maintain its critical taper.

This wedge behavior may be illustrated on the laboratory scale using a simple mechanical model [Davis, 1978]. The model consists of sand contained in a bottomless box with transparent side walls that sits upon a sheet of Mylar, which in turn lies on a flat rigid base (Figure 2). In most sandbox deformational models, horizontal compression is induced by pushing one wall of the model. Here, the same effect is achieved by pulling the Mylar sheet upon which the sand rests; this pulls the sand against the back wall of the model, which serves as a rigid buttress. The apparatus mimics the process of plate subduction and allows large deformation with mechanical simplicity. Inhomogeneities are minimized by packing the sand evenly, and side wall friction is effectively reduced by coating with graphite.

A sequence of photographs of one experimental run is shown in Figure 3. As deformation progresses, the wedge thickens and the locus of active deformation moves away from the rigid buttress until the taper reaches its steady state critical value. The wedge then slides stably. If sand continues to be accreted at the toe, the wedge continues to grow, maintaining its critical taper. Quantitative aspects of these experiments are discussed later in this paper.

We choose to model fold-and-thrust belts and accretionary wedges as critically tapered deforming wedges of rock analogous to the wedge of homogeneous sand in the experiment. Such a model is intended, of course, only to represent the gross macroscopic mechanics and not the complex internal structural details or deformational histories of specific wedges. In the case of an accretionary wedge in front of an island arc, the bulldozer represents the lithospheric plate beneath which oceanic crust is being subducted, and in the case of a fold-and-thrust belt, it represents the inner thicker part of the mountain range. We should also note that a metal bulldozer is made of much stronger material than the material it pushes; this is not true in the earth, in which rigid, less easily deformed segments of the lithosphere are generally stronger largely because they are thicker.

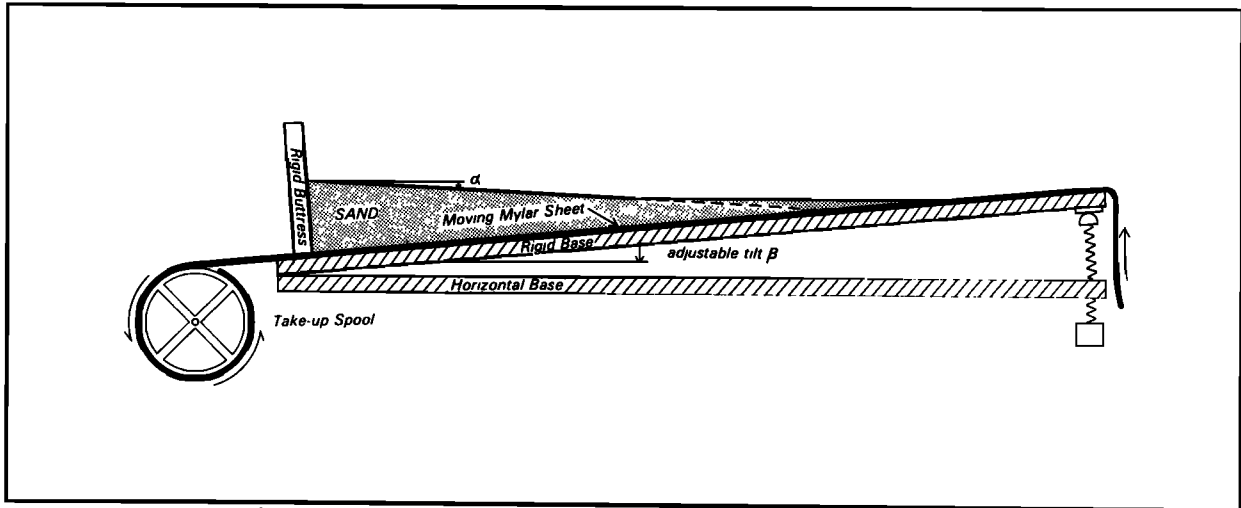


Fig. 2. Schematic diagram of laboratory sandbox model of Coulomb wedge. Underlying Mylar sheet is pulled out beneath buttress at left.

PROPERTIES OF THE MODEL

A fundamental premise of the present model is that rock deformation in the upper lithosphere is governed by pressure-dependent, time-independent Coulomb behavior, i.e., by brittle fracture [Paterson, 1978] or frictional sliding [Byerlee, 1978]. Macroscopically, the empirical law describing both these modes of brittle behavior is the same, only differing in the numerical value of the cohesive strength S_0 and the coefficient of friction $\mu = \tan \phi$, which expresses the pressure dependence. The general Coulomb criterion for shear traction τ at failure is of the form

$$|\tau| = S_0 + \mu(\sigma_n - p_f) \tag{1}$$

where σ_n is the normal traction and p_f is the pore fluid pressure.

Cohesion S_0 is relatively unimportant in the mechanics of fold-and-thrust belts and accretionary wedges that are composed predominantly of silicate sediments. Typical laboratory measurements of S_0 from fracture experiments on small samples of shales and sandstones range from 5 to 20 MPa [Hoshino et al., 1972], which is several times less than the cohesion of granites and other stronger rocks. In addition, these measurements probably overestimate the cohesive strengths of in situ rock masses because they are commonly done on relatively pristine samples and because rock strength decreases with larger samples containing more flaws. At depths on the order of a few kilometers the effect of this relatively small cohesion is negligible in comparison with the pressure-dependent term in the failure equation (see Figure 6a, below, for an illustration). The main effects of cohesion on wedge geometry will be observed near the toe of the wedge, where cohesion can add significantly to the total strength and produce a critical taper narrower than the corresponding cohesionless taper. Farther from the toe where the wedge is thicker, the pressure-dependent term will dominate, and the critical taper will asymptotically approach the cohesionless value. For simplicity we shall ignore the effect of cohesion on toe shape entirely in this paper and employ instead of (1) a noncohesive failure law of the form

$$|\tau| = \mu\sigma_n^* \tag{2}$$

Here, as well as elsewhere in this paper, we have used an asterisk to denote the effective stress $\sigma_n^* = \sigma_n - p_f$.

Pore fluid pressures p_f play a major role in the mechanics of thrust faulting [Hubbert and Rubey, 1959], and a proper accounting of their effect in both subaerial and submarine wedges requires some care. It is common in the subaerial case to assume that the water table is located at the rock surface (Figure 4a). The pore water pressure is in that case typically equal to the hydrostatic pressure for shallow depths. However, below some point whose location is stratigraphically controlled, it often rises well above the hydrostatic pressure, typically attaining a constant gradient somewhere in the range between the hydrostatic and the lithostatic gradient [Fertl, 1976]. This gradient is commonly described in terms of Hubbert and Rubey's dimensionless parameter λ , the ratio of pore fluid pressure p_f to the vertical normal traction exerted by the lithostatic overburden.

In many regions the water table may be located below the upper surface of the rock (Figure 4b). Fluid pressures are in that case reduced, and the rock will be relatively stronger. A third circumstance is that which arises in dealing with accretionary wedges: the rock surface in that case is submerged below sea level (Figure 4c). Rocks just below the seafloor will generally be quite weak, since the effective lithostatic pressure there always vanishes. To deal with this submarine case it is necessary to introduce a slight generalization of Hubbert and Rubey's subaerial λ , and that is done below; see (6).

The lower limit of applicability of the present brittle wedge theory is the middle or lower crust where pressure and temperature become sufficiently high that common rocks begin to display temperature-dependent plastic behavior, deforming by motion of dislocations and other pressure-independent mechanisms. The expected effects of this brittle-plastic transition on the geometry of large wedges are discussed further at the end of this paper.

THEORETICAL ESTIMATION OF CRITICAL TAPER

Consider a homogeneous wedge of deformable noncohesive Coulomb material being compressed by a push from its thick end, sliding along a rigid base (Figure 5). Let α be the

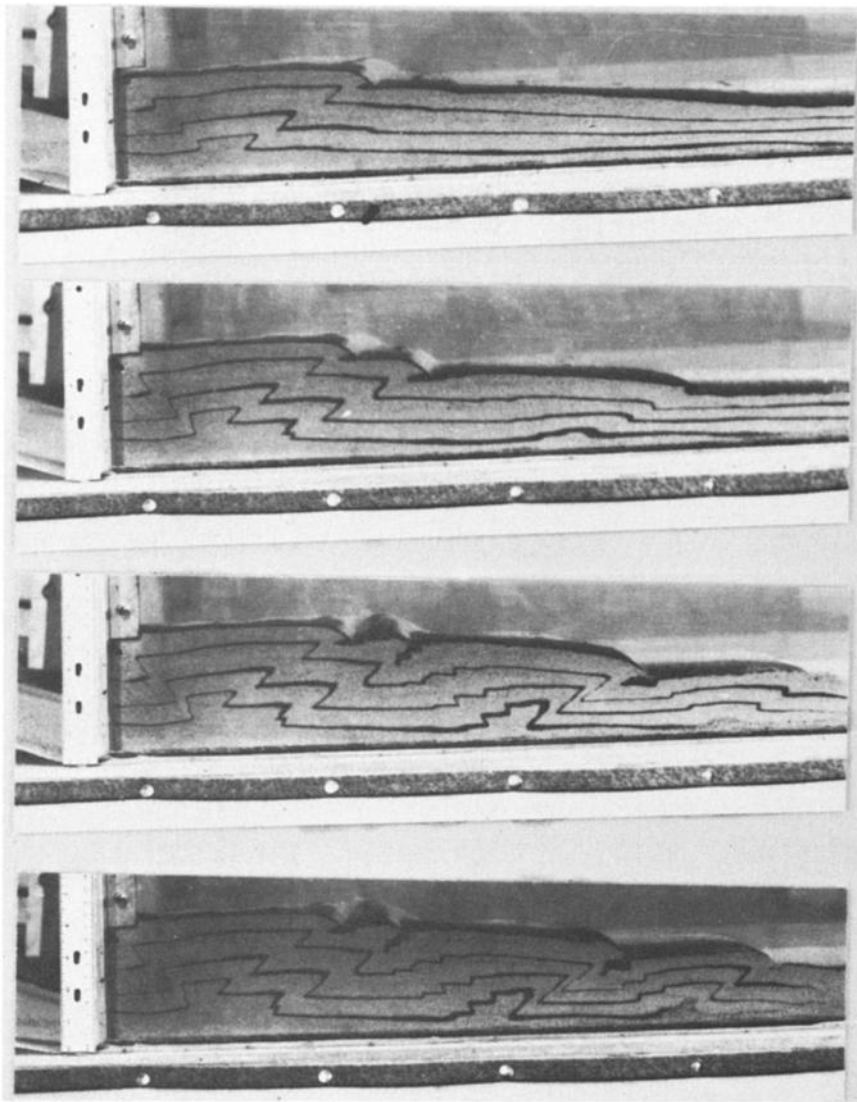


Fig. 3. Photographic side view of stages in deformation of sand during an experimental run. Initially undeformed sand mass is increasingly compressed and deformed by thrusting until the critical taper is attained. Black sand layers are passive markers.

local angle of topographic relief and β be the local dip angle of the rigid base, as shown. A system of local Cartesian coordinates x, z will be employed, having x parallel to the base in the segment of the wedge between x and $x + dx$ and with z increasing upward. The local thickness of the wedge, measured along the z axis, will be denoted by H . In the case of a submarine wedge the local thickness of the water overburden, measured along the direction of gravity, will be denoted by D .

The critical taper of such a horizontally compressive wedge is governed essentially by the balance of forces in the x direction. Let us enumerate the forces acting on the segment of unit length along strike (i.e., in and out of the page) lying between x and $x + dx$. There is, first, a gravitational body force whose x component is $-\rho g H dx \sin \beta$ where ρ , assumed constant, is the density of the rocks in the wedge and g is the acceleration of gravity. Second, in the case of a submarine wedge there is another force arising directly from gravity, namely, the pressure of the water overburden, which has an x component $-\rho_w g D dx \sin (\alpha +$

$\beta)$ where ρ_w is the density of water. For greater generality we shall consider explicitly the case of a submarine wedge in the analysis that follows, with the knowledge that the corresponding result for the subaerial case may be recovered at any point in the argument by setting ρ_w equal to zero (or more precisely to the density of air, which is negligible). The third force, which acts on both subaerial and submarine wedges, is the frictional resistance to sliding along the basal decollement. In terms of the basal shear traction τ_b this force is $-\tau_b dx$, the minus sign arising because the force acts to resist sliding. Finally, let σ_x be the normal traction acting across any face perpendicular to the x axis, with compression being reckoned positive. The fourth force acting on the segment between x and $x + dx$ is then the resultant compressive push of these normal tractions acting on the two side walls. In contrast to the first three forces, this resultant is the $+x$ direction, for two reasons: not only is the x face larger in area than that at $x + dx$, but because the push is coming from the thick end, $\sigma_x(x, z)$ exceeds $\sigma_x(x + dx, z)$. Balancing forces requires in the limit $dx \rightarrow 0$ that

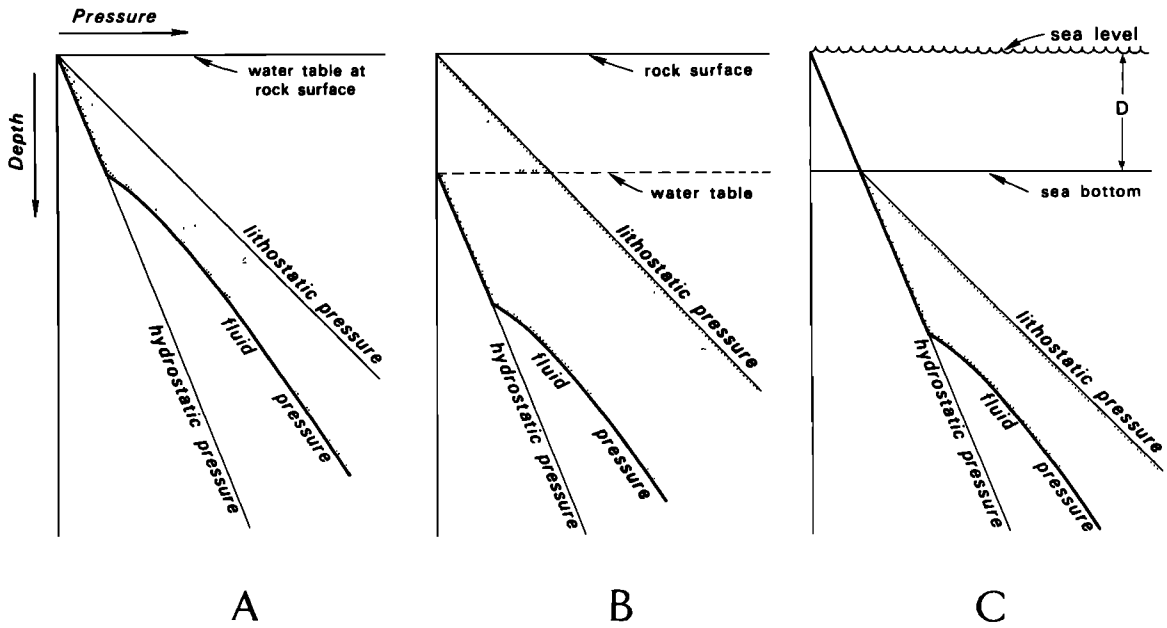


Fig. 4. Relationship between fluid pressure p_f and vertical normal traction σ_z in three cases: (a) water table at surface; (b) water table below surface; (c) rock submerged. In all three cases the Coulomb shear strength is proportional to the difference $\sigma_z^* = \sigma_z - p_f$, shown by shading.

$$\rho g H \sin \beta + \rho_w g D \sin (\alpha + \beta) + \tau_b + \frac{d}{dx} \int_0^H \sigma_x dz = 0 \quad (3)$$

The thin-skinned nature of actual wedges allows us, with very little error, to make use of a small-angle approximation in which $\sin \alpha \approx \alpha$ and $\sin \beta \approx \beta$. With this substitution, (3) reduces to the simpler form

$$\rho g H \beta + \rho_w g D (\alpha + \beta) + \tau_b + \frac{d}{dx} \int_0^H \sigma_x dz = 0 \quad (4)$$

The vertical normal traction, σ_z , at any point in the wedge will be assumed to be solely that due to the lithostatic and hydrostatic overburden, i.e.,

$$\sigma_z = \rho_w g D + \rho g (H - z) \quad (5)$$

This assumption also depends for its validity on a small-angle approximation. By defining a dimensionless quantity

$$\lambda = \frac{p_f - \rho_w g D}{\sigma_z - \rho_w g D} \quad (6)$$

we may write the effective normal traction $\sigma_z^* = \sigma_z - p_f$ in the form

$$\sigma_z^* = (1 - \lambda) \rho g (H - z) \quad (7)$$

Equation (6) provides the appropriate generalization to the case of a submarine wedge of the pore fluid pressure ratio $\lambda = p_f/\sigma_z$ of Hubbert and Rubey. In essence the hydrostatic pressure at the seafloor, $\rho_w g D$, has been adopted as a reference level; inspection of Figures 4a and 4c makes it clear that this is a logical procedure.

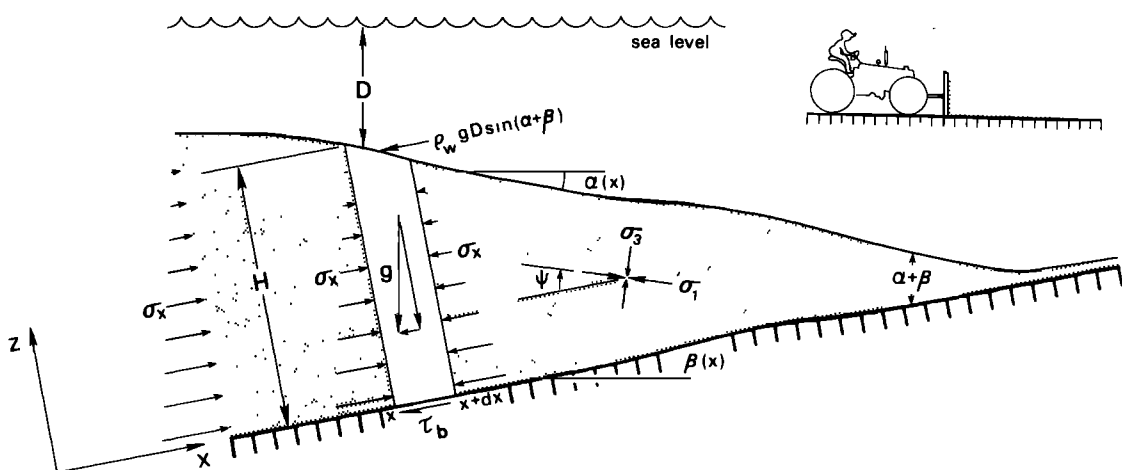


Fig. 5. Schematic diagram of a wedge of material subject to horizontal compression and on the verge of Coulomb failure throughout. The force balance on an arbitrary column of width dx is shown and the terminology used in deriving the equations of critical taper is indicated.

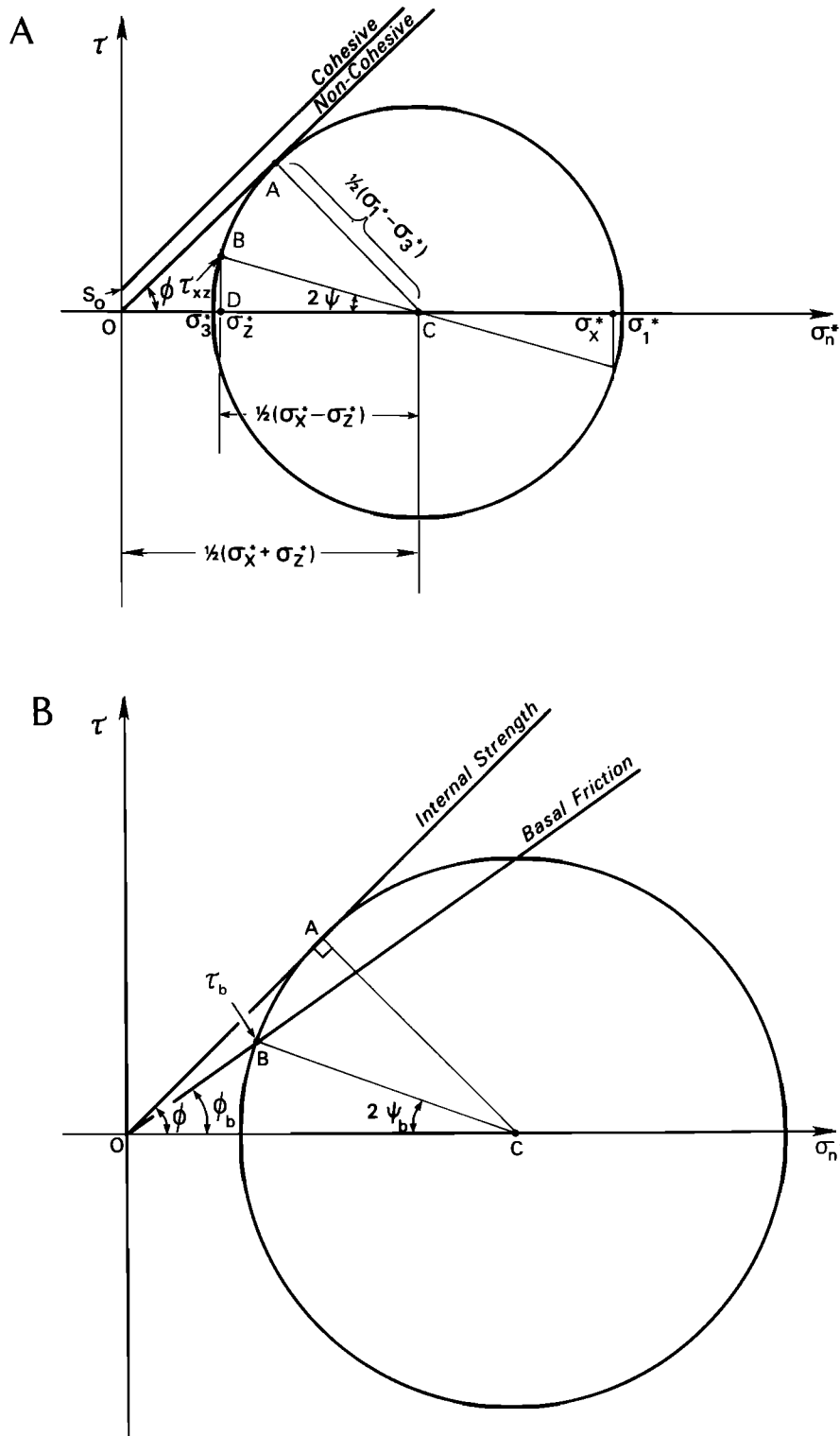


Fig. 6. Mohr diagram illustrating the state of stress (a) at some point within the wedge and (b) at the base of the wedge. The quantities ϕ and ϕ_b are the angles of internal and basal friction, and ψ and ψ_b are the angles between σ_1 and the x axis within the wedge and at the base of the wedge. The basal shear traction τ_b is given by the intersection of the frictional failure law $|\tau| = \mu_b \sigma_n^*$ with the Mohr stress circle corresponding to the basal depth H .

The traction τ_b resisting frictional sliding on the base will be written as

$$\tau_b = \mu_b \sigma_z^* = \mu_b (1 - \lambda_b) \rho g H \quad (8)$$

where $\mu_b = \tan \phi_b$ is the basal coefficient of friction and λ_b is the generalized Hubbert-Rubey ratio (6) on the base. In introducing the basal values μ_b and λ_b we allow explicitly for

the fact that the basal decollement will usually be a zone of weakness, either because of a lower intrinsic strength or because of elevated fluid pressures. For a wedge with uniform internal properties μ and λ , we must necessarily have $(1 - \lambda_b)\mu_b \leq (1 - \lambda)\mu$ for the base of the wedge to be a throughgoing decollement.

To determine the remaining unknown quantity σ_x in the

force-balance equation (4), we must consider the state of stress within the wedge in more detail. A Mohr-circle representation of the stress at an arbitrary point is shown in Figure 6a. The maximum and minimum effective compressive stresses have been denoted by σ_1^* and σ_3^* , respectively. The local angle between the axis of maximum compressive stress and the x axis will be denoted by ψ (see Figure 5). Since a critically tapered wedge is assumed to be on the verge of shear failure throughout, there will be at every point two planes oriented at angles $\pm(\pi/4 - \phi/2)$ with respect to the σ_1 axis on which the failure criterion $|\tau| = \mu\sigma_n^*$ is satisfied [Jaeger and Cook, 1969]. By inspection of triangle BCD in Figure 6a we see that

$$\frac{1}{2}(\sigma_x^* - \sigma_z^*) = \frac{1}{2}(\sigma_1^* - \sigma_3^*) \cos 2\psi \quad (9)$$

whereas from triangle OAC we find

$$\frac{1}{2}(\sigma_1^* - \sigma_3^*) = \frac{1}{2}(\sigma_x^* + \sigma_z^*) \sin \phi \quad (10)$$

Combining these expressions, we find the stress difference $\frac{1}{2}(\sigma_x - \sigma_z) = \frac{1}{2}(\sigma_x^* - \sigma_z^*)$ to be

$$\frac{1}{2}(\sigma_x - \sigma_z) = \frac{\sigma_z^*}{\csc \phi \sec 2\psi - 1} = \frac{(1 - \lambda)\rho g(H - z)}{\csc \phi \sec 2\psi - 1} \quad (11)$$

This equation together with the corresponding result for the shear stress

$$\tau_{xz} = \frac{1}{2}(\sigma_x - \sigma_z) \tan 2\psi = \frac{(1 - \lambda)\rho g(H - z) \tan 2\psi}{\csc \phi \sec 2\psi - 1} \quad (12)$$

completely define the state of plane stress within a noncohesive critical Coulomb wedge in terms of a single parameter, the stress orientation angle ψ .

Upon combining (5) and (11) we are now able to write the integral appearing in the force balance equation (4) in the form

$$\int_0^H \sigma_x dz = \rho_w g D H + \frac{1}{2} \rho g H^2 + 2\rho g \int_0^H \frac{(1 - \lambda)(H - z)}{\csc \phi \sec 2\psi - 1} dz \quad (13)$$

Invoking the small-angle approximation once again, we set

$$dH/dx = -(\alpha + \beta) \quad (14)$$

$$dD/dx = \alpha \quad (15)$$

so that

$$\frac{d}{dx} \int_0^H \sigma_x dz = \rho_w g H \alpha - \rho_w g D(\alpha + \beta) - \rho g H(\alpha + \beta) - 2\rho g(\alpha + \beta) \int_0^H \frac{(1 - \lambda)}{\csc \phi \sec 2\psi - 1} dz \quad (16)$$

In writing (16) we have assumed that all of λ , ϕ , and ψ are independent of x , but they may all in general still depend upon depth z . For simplicity, however, we shall henceforth consider both λ and ϕ to be strictly constant, regarding them as the averaged or effective values for the wedge as a whole.

Even in a wedge with uniform properties the angle ψ will vary appreciably with depth, particularly if $\lambda_b \approx \lambda$ and $\mu_b \approx \mu$.

For convenience, after removing the factor of $(1 - \lambda)$ from under the integral sign in (16), let us define a dimensionless quantity

$$K = 2H^{-1} \int_0^H \frac{dz}{\csc \phi \sec 2\psi(z) - 1} \quad (17)$$

When (8) and (16) are substituted into (4), we find the theoretical critical taper $\alpha + \beta$ of a noncohesive Coulomb wedge to be

$$\alpha + \beta = \frac{(1 - \lambda_b)\mu_b + (1 - \rho_w/\rho)\beta}{(1 - \rho_w/\rho) + (1 - \lambda)K} \quad (18)$$

It is noteworthy that this equation contains no explicit dependence on x so that a wedge with uniform properties and a planar base should have a constant surface slope. Note, in addition, that in the limit $\lambda_b \rightarrow \lambda \rightarrow 1$, (18) reduces to $\alpha \rightarrow 0$, which is the expected result for a wedge composed of material having negligible strength. For future reference, we remark that (18) defines a linear relationship between α and β of the form

$$\alpha + R\beta = F \quad (19)$$

where

$$R = \frac{(1 - \lambda)K}{(1 - \rho_w/\rho) + (1 - \lambda)K} \quad (20)$$

$$F = \frac{(1 - \lambda_b)\mu_b}{(1 - \rho_w/\rho) + (1 - \lambda)K} \quad (21)$$

To determine the quantity K exactly, we must know the angle $\psi(z)$ at every depth in the wedge $0 \leq z \leq H$ and this cannot be found entirely analytically. In a forthcoming paper, we will show how $\psi(z)$ can be found numerically by a very straightforward and rapid procedure, in both the case of a noncohesive wedge as well as one with a finite cohesion S_0 . In the present paper we shall employ instead a simple analytical approximation to K , which we have tested thoroughly against our exact noncohesive numerical results and found to be extremely accurate. To develop this approximation, we shall, for the moment, assume that $\lambda_b = \lambda$; the wedge existence condition is in that case simply $\mu_b \leq \mu$ and the critical taper equation (18) reduces to

$$\alpha + \beta = \frac{(1 - \lambda)\mu_b + (1 - \rho_w/\rho)\beta}{(1 - \rho_w/\rho) + (1 - \lambda)K} \quad (22)$$

We note first that at the top surface of the wedge, if there is the slightest cohesion, σ_1 must be parallel to the local topography so that $\psi_t = \psi(H) = \alpha + \beta$. In the small-angle approximation $\alpha + \beta \ll 1$ the integrand in (17) near the top of the wedge can thus be replaced by

$$\frac{1}{\csc \phi \sec 2\psi_t - 1} = \frac{\sin \phi}{1 - \sin \phi} \quad (23)$$

The angle $\psi_b = \psi(0)$ near the base of the wedge can be found from the specification that frictional sliding governed by a coefficient of friction μ_b is occurring there; a Mohr-circle representation of the basal state in the case $\lambda_b = \lambda$ and

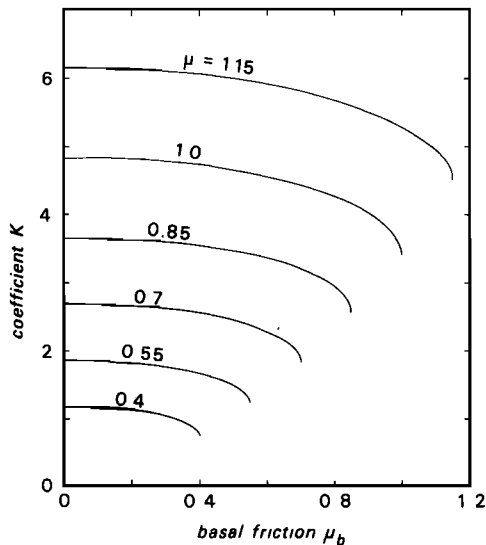


Fig. 7. Sensitivity of coefficient K to basal and apparent internal coefficients of friction μ_b and μ . If μ_b is small in comparison with μ , $K \approx 2 \sin \phi / (1 - \sin \phi)$, but as $\mu_b \rightarrow \mu$, K decreases significantly and in fact $\partial K / \partial \mu_b \rightarrow -\infty$.

$\mu_b < \mu$ is shown in Figure 6b. By applying the law of sines to the two triangles OAC and OBC it may be shown that

$$\psi_b = \frac{\pi}{4} - \frac{\phi_b}{2} - \frac{1}{2} \arccos \left(\frac{\sin \phi_b}{\sin \phi} \right) \quad (24)$$

and, after some algebra,

$$\frac{1}{\csc \phi \sec 2\psi_b - 1} = \frac{\sin^2 \phi_b + \cos \phi_b (\sin^2 \phi - \sin^2 \phi_b)^{1/2}}{\cos^2 \phi_b - \cos \phi_b (\sin^2 \phi - \sin^2 \phi_b)^{1/2}} \quad (25)$$

In the limiting case $\phi_b \rightarrow \phi$

$$\frac{1}{\csc \phi \sec 2\psi_b - 1} \rightarrow \tan^2 \phi_b \quad (26)$$

If on the other hand the basal layer is very weak, i.e., $\phi_b \ll \phi$, then $\psi(z)$ is small everywhere and

$$\frac{1}{\csc \phi \sec 2\psi_b - 1} = \frac{\sin \phi}{1 - \sin \phi} \quad (27)$$

To obtain an approximate expression for K valid in either limit, we approximate the integrand in the interval $0 \leq z \leq H$ by a linear function passing through the two end points (23) and (25); this leads to

$$K \approx \frac{\sin \phi}{1 - \sin \phi} + \frac{\sin^2 \phi_b + \cos \phi_b (\sin^2 \phi - \sin^2 \phi_b)^{1/2}}{\cos^2 \phi_b - \cos \phi_b (\sin^2 \phi - \sin^2 \phi_b)^{1/2}} \quad (28)$$

This, together with (22), can be used to find the theoretical critical taper $\alpha + \beta$ of an actively deforming Coulomb wedge with prescribed physical properties μ , μ_b , and $\lambda_b = \lambda$. The nature of the variation of K with μ and μ_b is illustrated in Figure 7. An increase in basal friction increases the critical taper because of the factor μ_b in the numerator of (22), but an increase in the effective internal friction leads to a decrease in the critical taper, since K is an increasing

function of μ for fixed μ_b . An internally stronger wedge can be narrower and still undergo stable sliding without deforming. To obtain an approximation valid in the case $\lambda_b \neq \lambda$, it is necessary to replace ϕ_b in (28) by $\arctan [\phi_b(1 - \lambda_b)/(1 - \lambda)]$. In all of the specific comparisons with laboratory and field observations considered below we have in fact assumed that $\lambda_b = \lambda$, so that the simpler forms (22) and (28) are pertinent.

Before considering any applications of the critical taper formulae (18) and (28), it is of interest to point out another more fundamental form of the force balance in a critical wedge, obtained by inserting (16) into (4). This leads to a formula for the basal shear traction τ_b , namely,

$$\tau_b = (\rho - \rho_w)gH\alpha + (1 - \lambda)K\rho gH(\alpha + \beta) \quad (29)$$

This equation shows that the frictional sliding resistance on the base is counteracted by two terms, both of which may be thought of as driving forces responsible for the tectonic deformation and overthrusting. The first term is due to gravity acting on the sloping top surface of the wedge and is the same as that which causes a glacier to slide in the direction of its surface slope regardless of the attitude of its bed. This term has been discussed in the context of gravity sliding or spreading models of overthrust tectonics by Elliott [1976]. The effective density $\rho - \rho_w$ appears naturally in (30) in the case of a submarine wedge, as expected on intuitive grounds. The second term depends on the taper $\alpha + \beta$ and is a consequence of the horizontally compressive push assumed to be acting from the rear of the wedge. For typical silicate sedimentary accretionary wedges with geologically reasonable values of μ , μ_b and $\lambda = \lambda_b$, this second term is larger than the first by a factor of 4 to 5, which implies that basal shear tractions in compressive, critically tapered wedges are larger by the same factor than those estimated by Elliott [1976].

At this point in our discussion it is also appropriate to indicate the relationship between our analysis and the well-known Hubbert and Rubey [1959] analysis of the maximum possible lengths of thrust sheets. To illustrate the effect of fluid pressure on thrust faulting, they computed the maximum length of a rectangular body ($\alpha + \beta = 0$), of a given

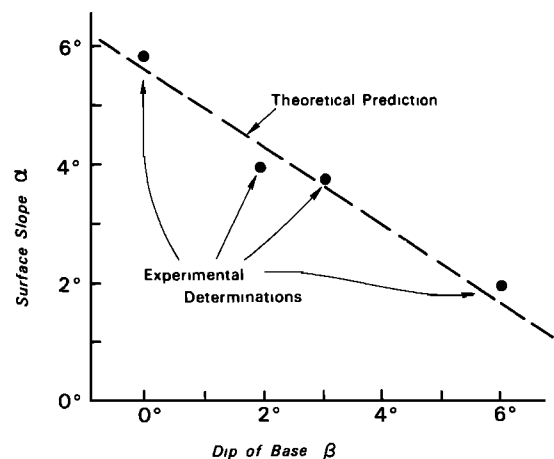


Fig. 8. Mean surface slope measured by linear regression off photographs versus dip of rigid base in sandbox experiments. Dots represent the average of eight experimental runs at $\beta = 0^\circ$, two at $\beta = 2^\circ$, fourteen at $\beta = 3^\circ$, and nine at $\beta = 6^\circ$. Line is theoretical prediction $\alpha = 5.9^\circ - 0.66\beta$.

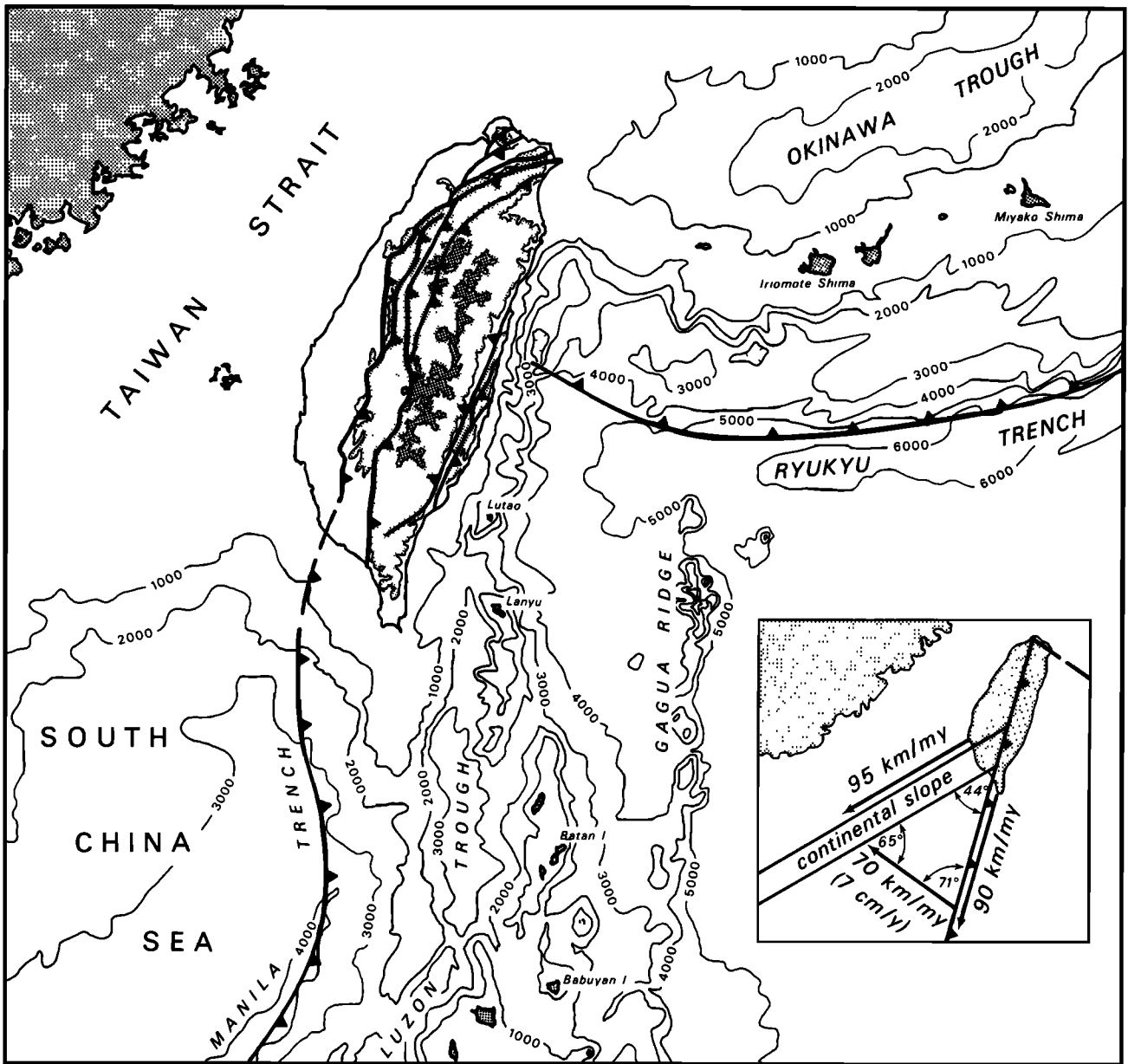


Fig. 9. Tectonic and bathymetric setting of Taiwan with velocity triangle for arc-continent collision in Taiwan assuming plate motions of Seno [1977].

thickness, that can be pushed along a basal decollement without undergoing internal Coulomb failure. Their analysis is appropriate to the immediate vicinity of the toe of a deforming wedge, where flat-lying sediments are being accreted. A thrust sheet longer than the Hubbert-Rubey maximum deforms by thrusting and thickening toward its rear until its geometry is that of a critically tapered wedge. The once perplexing mechanical problems posed by the existence of large-scale thrust sheets and fold-and-thrust belts are, in a sense, an artifact of imposing a fixed rectangular geometry; this point has been emphasized by Chapple [1978] also. Whereas Hubbert and Rubey calculated the maximum length overthrust attainable without a taper, we calculate the critical taper required for the emplacement of a thrust sheet of any length. A more quantitative comparison of our results and theirs, including the role of cohesion, will be published elsewhere.

EXPERIMENTAL VERIFICATION WITH LABORATORY SANDBOX MODEL

In the sandbox experiment described above (Figures 2 and 3) the sand was dry ($\lambda = 0$); therefore the equation for the critical taper (22) reduces to

$$\alpha + \beta = \frac{\mu_b + \beta}{1 + K} \quad (30)$$

Loosely packed dry sand is a Coulomb material exhibiting negligible cohesion and an angle of internal friction near $\phi = 30^\circ$, corresponding to $\mu = 0.58$ [Lambe and Whitman, 1979]. We measured the coefficient of friction of sand on Mylar to be $\mu_b = 0.30$ by experimentally observing the inclination required to initiate gravitational sliding of a confined cylinder of sand resting on a Mylar surface. From (28) we find the value of K corresponding to $\mu = 0.58$ and $\mu_b = 0.30$ to be K

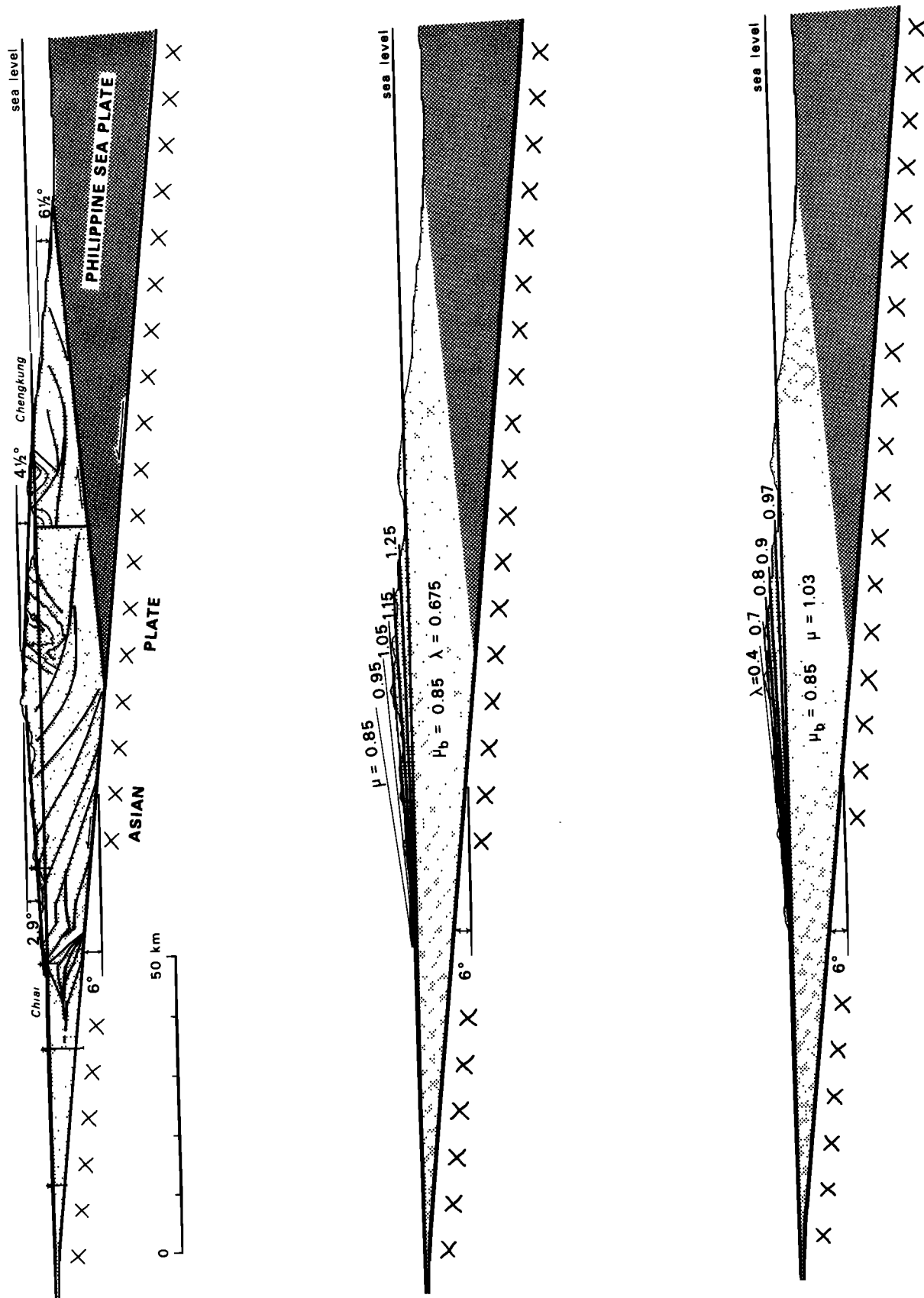


Fig. 10. Regional tectonic cross section of south-central Taiwan near Chiai oriented N20°E. Based on data of Suppe [1980b, 1981], Stanley *et al.* [1981], and Chi *et al.* [1981]. The regional surface slope of 2.9° in western Taiwan is well explained by the critical Coulomb wedge theory with $\mu_b = 0.85$, $\mu = 1.03$, and $\lambda \approx 0.7$. The sensitivity to μ with the fluid pressure ratio fixed at the observed value $\lambda = 0.675$ is greater than the sensitivity to λ for fixed μ .

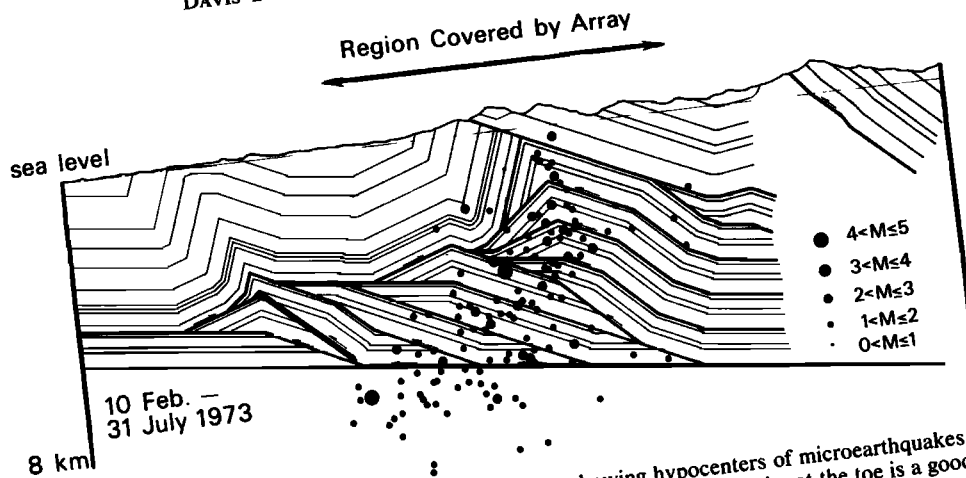


Fig. 11. Toe of active western Taiwan fold-and-thrust belt, showing hypocenters of microearthquakes near cross section in foothills of southern Taiwan [after Suppe, 1980b; Wu *et al.*, 1979]. Seismicity at the toe is a good indication that the interior of the wedge is at or near its critical taper.

= 1.92. The relation between α and β predicted by the theory is then

$$\alpha = 5.9^\circ - 0.66\beta \quad (31)$$

This prediction is confirmed by the experimentally determined result that (Figure 8)

$$\alpha = (5.7^\circ \pm 0.2^\circ) - (0.66 \pm 0.14)\beta \quad (32)$$

Experiments using graphite and sandpaper on the base produced substantially smaller and larger tapers [Davis, 1978; Goldburg, 1982], which is also in accord with the theory.

Neither (18) nor (28) contains any length scale; therefore the theory for noncohesive Coulomb wedges is inherently scale independent. Given this, the success of the theory in describing the behavior of our controlled laboratory model and the low cohesive strengths of sedimentary rocks, as discussed above, we are encouraged to consider applications to more complicated geological cases.

APPLICATION OF THE THEORY TO TAIWAN

Tectonic Setting

Taiwan is an actively deforming mountain belt situated on the continental shelf of China at the western edge of the Philippine Sea plate (Figure 9). The Asian plate is subducting beneath the Philippine Sea plate along the Manila Trench and western Taiwan foothills in the segment of the plate boundary between Luzon and northern Taiwan (Figure 10). In contrast, the subduction is of opposite polarity both to the north along the Ryukyu trench and to the south along the Mindanao trench [Seno, 1977; Tsai *et al.*, 1977; Wu, 1979]. The convergence between the Asian and the Philippine Sea plates near Taiwan is estimated by Seno [1977] to be about 7 cm/yr in a northwest-southeast direction.

It is noteworthy that the plate boundary cuts across the continent-ocean boundary in the Taiwan-Luzon region; the Luzon Arc and Manila Trench are oriented north-south, whereas the stable continental margin of China southwest of Taiwan is oriented northeast-southwest. This geometry results in an oblique collision between the Luzon Arc and the Chinese continental margin (see Figure 9). The collision began about 4 m.y. ago in northernmost Taiwan [Chi *et al.*, 1981], is occurring now just south of Taiwan, and will occur

in the future between Luzon and Hong Kong. As the plate boundary impinges in turn on the thick sedimentary sequences of the Chinese continental rise, slope, and shelf, the accretionary wedge expands continuously in width and height to become the Central Mountains of Taiwan rising nearly 4 km above sea level. Once the accretionary wedge rises above sea level, it is no longer able to grow unobstructedly because of the high erosion rate, which reaches 5 to 6 km/m.y. [Li, 1976]. In fact, the topography of the mountain belt in central Taiwan has achieved a steady state in which tectonic compression is balanced by erosion [Suppe, 1981]. Taiwan in this region is an active foreland fold-and-thrust belt with present-day deformation extending into the toe as evidenced by seismic activity (see Figure 11). These observations show that the interior of the mountain belt is at critical taper. The existence of a large amount of structural and fluid pressure information collected during the course of petroleum exploration and production in addition to the active deformation and steady state topography make western Taiwan a particularly appropriate place to test our theory of the critical taper of a subaerial wedge.

Surface Slope

Topographic profiles of central Taiwan show that the mountains have very nearly a constant surface slope, except for small topographic features such as ridges and valleys on a scale of 5 km or less. Best fit linear regressions to the western slope of Taiwan vary between 2.5° and 3.4° (Figure 12) with the mean slope being $\alpha = 2.9^\circ \pm 0.3^\circ$. This is a remarkably constant surface slope over a fairly large area, suggesting that the entire region has homogeneous material properties, fluid pressure, and decollement slope, as well as a close approach to the critical taper.

Decollement Dip

The regional dip of the basal decollement in western Taiwan is of course not as easily measured as the regional surface slope, but it has been fairly well determined in the frontal part of the wedge by seismic reflection profiling, deep drilling, and the construction of retrodeformable geologic cross sections [Suppe, 1980a, b, 1981; Suppe and Namson, 1979; Namson, 1982]. The area of well-constrained dip in Figure 10 extends from the deformational front located near

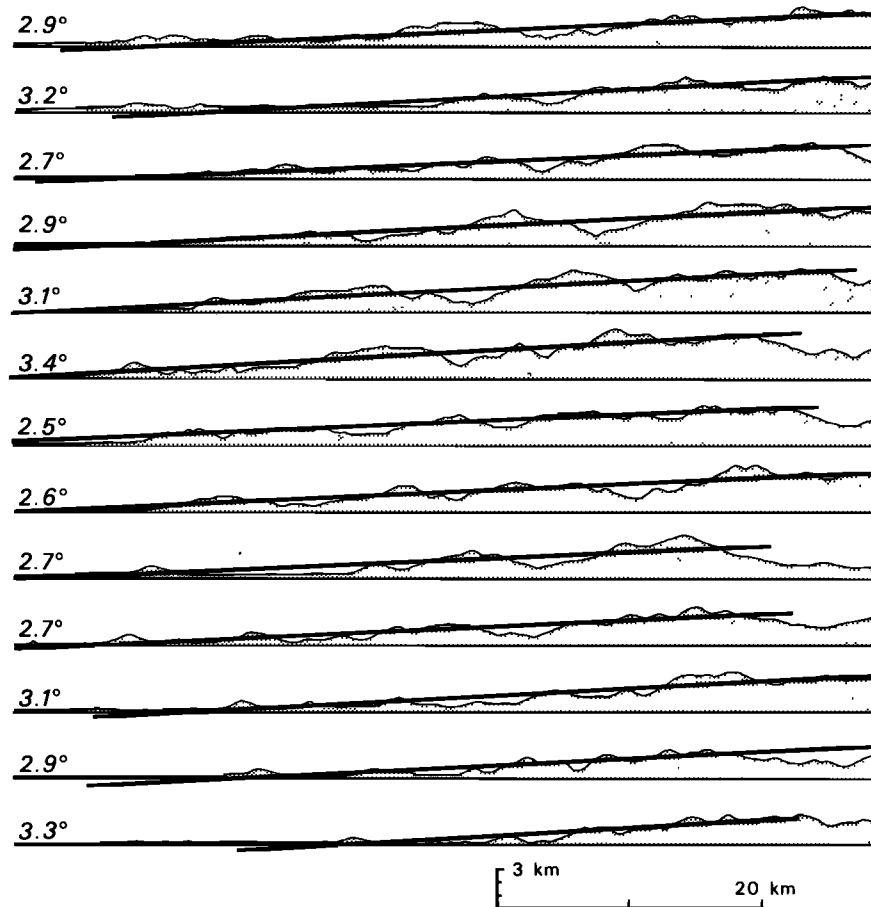


Fig. 12. Topographic profiles of western slope of central Taiwan in the region of steady state topography (see Suppe [1981] for locations). In all cases the topography can be well fit by a constant-slope regression. The mean slope of the set of profiles is $\alpha = 2.9^\circ \pm 0.3^\circ$.

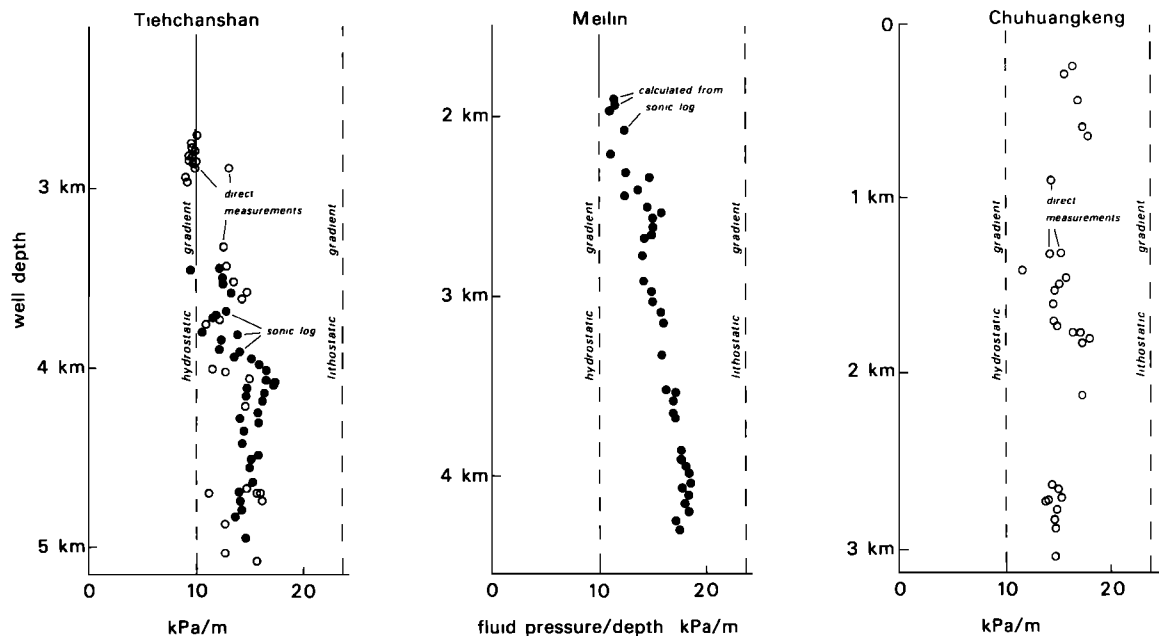


Fig. 13. Observed fluid pressure/depth as a function of depth in three areas of western Taiwan [Suppe and Wittke, 1977; Suppe et al., 1981]. The Tiehchanshan and Meilin areas are at the edge of the overthrust belt and have undergone little erosion. They display a permeable hydrostatic zone overlying the less permeable overpressured rocks. The Chuhuangkeng area is deeper in the fold-and-thrust belt, it has undergone more erosion, and overpressured fluid pressure gradients reach essentially to the surface. It is considered typical of the mountainous areas of western Taiwan. The overpressured values correspond to $\lambda \approx 0.7$ in these three areas and elsewhere in western Taiwan.

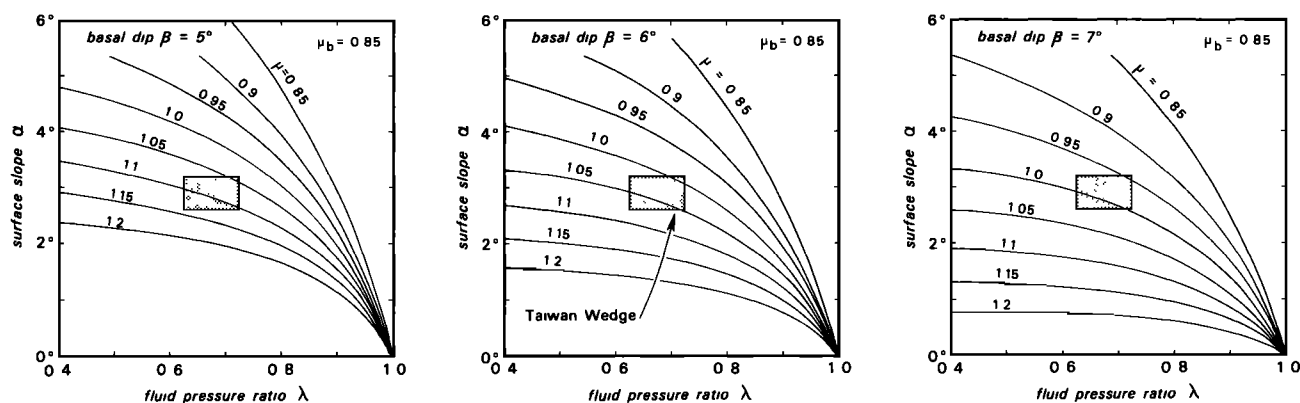


Fig. 14. Surface slope α versus fluid pressure ratio λ for three basal dips $\beta = 6^\circ \pm 1^\circ$, with Byerlee's law $\mu_b = 0.85$ assumed on the basal decollement. Shaded box shows measured α and $\lambda = \lambda_b$ in western Taiwan. The best fitting effective coefficient of internal friction is $\mu = 1.03$.

Chiai about 30 km into the wedge; the measured dip is $\beta = 6^\circ$ at the stratigraphic level of the basal decollement near the base of the Neogene continental margin section. At least in northern Taiwan it is known that this single level of decollement exists under the entire width of Taiwan [Suppe, 1980a]. We must extrapolate our 6° measurement in the toe region under the entire western slope of the mountains to obtain an estimate of the overall taper of the wedge. We believe that we know the decollement dip within $\pm 1^\circ$ everywhere and within $\pm 1/4^\circ$ many places near the toe.

Fluid Pressures

Fluid pressures are well known within the western foothills and coastal plain of Taiwan as a result of formation tests and sonic log measurements during petroleum exploration [Suppe and Wittke, 1977; Suppe et al., 1981]. Typical fluid pressure profiles at the western edge of the fold-and-thrust belt where there has been little erosion show an upper permeable zone of hydrostatic fluid pressure gradients ($\lambda \approx 0.4$) overlying less permeable sediments exhibiting overpressured fluid pressure gradients ($\lambda \approx 0.7$), as seen in the Tiehchanshan and Meilin wells in Figure 13. This overpressured gradient is very constant throughout western Taiwan. Very soon after the onset of deformation, the permeable Pliocene-Pleistocene sediments are eroded off the growing structures and overpressured fluid pressure gradients are exposed essentially at the surface of the wedge, as for example in the Chuhuangkeng field in Figure 13, which has Miocene rocks at the surface. Furthermore, major decollement surfaces that are intersected by deep drilling in the foothill zone show the same overpressured fluid pressure gradient as the overlying rocks [Suppe et al., 1981]. On the basis of all information we have available, we adopt a constant fluid pressure ratio $\lambda = \lambda_b = 0.675 \pm 0.05$ for both the wedge and decollement. It should be noted, however, that direct fluid pressure measurements are essentially restricted to the western third of the wedge.

Basal Friction

We have outlined the data on surface slope α , decollement dip β , and fluid pressure ratio $\lambda = \lambda_b$ in the preceding sections. The remaining parameters that enter into the critical taper of the mountain wedge are the coefficient of friction on the basal decollement μ_b and the corresponding effective coefficient of internal friction $\mu = \tan \phi$ within the

wedge. Neither of these is known from direct measurements in Taiwan. Laboratory studies have shown sliding friction to be remarkably uniform for a wide variety of rock types. According to Byerlee [1978], frictional sliding is well described by the relation $|\tau| = 0.85\sigma_n^*$ for effective normal tractions in the range 5–200 MPa, which encompasses most rocks above the brittle-plastic transition, especially in overpressured environments. In view of this laboratory evidence, we shall adopt Byerlee's empirical 'law' $\mu_b = 0.85$ on the basal decollement where it is logical to assume that essentially pure frictional sliding is occurring. We will then employ the critical Coulomb wedge theory, equations (22) and (28), to infer the effective coefficient of friction within the wedge, μ . This procedure yields our preferred model, but since there may be objections to the use of Byerlee's law on the base, we have in addition computed the complete range of values μ_b, μ consistent with the measured Taiwan field parameters $\alpha = 2.9^\circ, \beta = 6^\circ$, and $\lambda = \lambda_b \approx 0.7$.

Fitting the Theory to the Taiwan Data

The best-known parameter of the western Taiwan wedge is the surface slope $\alpha = 2.9^\circ$. In Figure 14 we show the theoretical surface slopes of critical Coulomb wedges having decollement dips $\beta = 6^\circ \pm 1^\circ$, plotted versus fluid pressure ratio λ for various values of μ , assuming Byerlee's law on the base. The best fitting value of the effective coefficient of internal friction is $\mu = 1.03$, about 20% greater than the assumed laboratory frictional value on the base. Given the uncertainties in α, β , and λ , and assuming that Byerlee's law is valid on the base, the uncertainty in μ is about 10%, so the inferred difference between μ and μ_b is real. An effective internal friction identical to the basal friction $\mu_b = 0.85$ is definitely precluded, since it would give rise to a surface slope $\alpha = 5.9^\circ$, assuming $\beta = 6^\circ$ and $\lambda = \lambda_b = 0.675$ (Figure 10). The implication of this difference between μ and μ_b is that, on the average, slightly larger shear tractions are required to produce internal deformation within the wedge than to permit frictional sliding along its base, which is a throughgoing decollement. We interpret this to mean that the wedge material is not so extensively fractured that preexisting slip planes of all possible orientations are available within it. Much of the internal deformation must be taken up by slip on suboptimally oriented surfaces; it is also likely that the commonly observed complex geological structures within the wedge may require fracturing for the deformation to

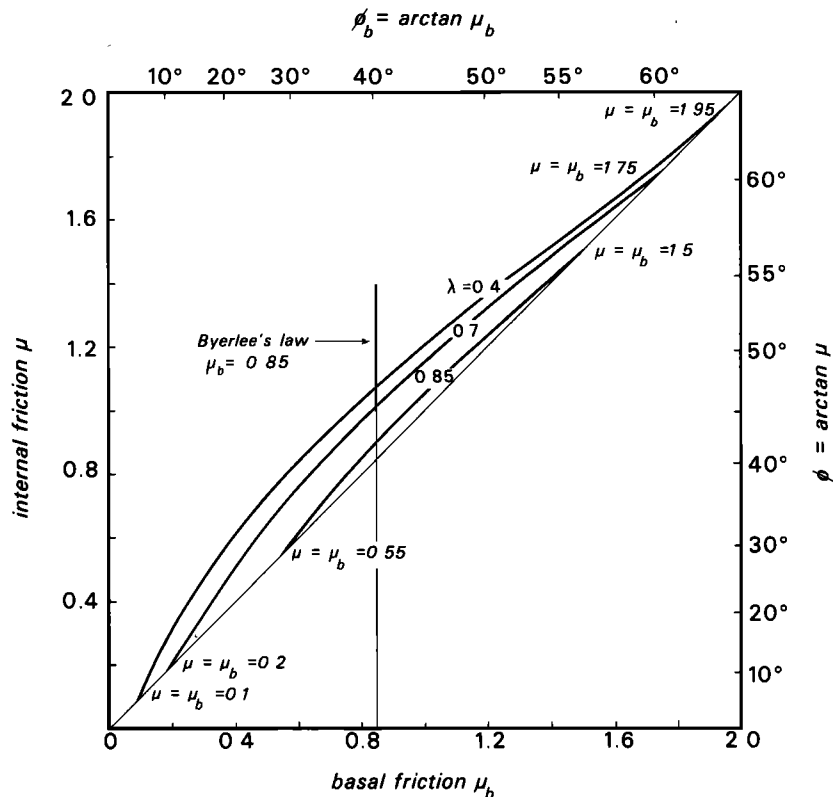


Fig. 15. Values of μ_b and μ consistent with the geometry of the western Taiwan fold-and-thrust belt, having $\alpha = 2.9^\circ$ and $\beta = 6^\circ$. For the measured fluid pressure ratio $\lambda \approx 0.7$, values between $\mu = \mu_b = 0.2$ and $\mu = \mu_b = 1.75$ can satisfy the data. With Byerlee's law $\mu_b = 0.85$ on the base, the effective coefficient of internal friction is $\mu = 1.03$. No solutions having $\mu < \mu_b$ are possible as long as $\lambda = \lambda_b$.

proceed. The ubiquitous presence throughout western Taiwan of fault-bend folds produced by the stepping up of faults from the basal decollement [Suppe, 1980b; Suppe and Namson, 1979; Namson, 1982] is consistent with this interpretation.

In conclusion, then, we find that the brittle rock strengths commonly measured in laboratory experiments are consistent with the observed regional topographic slope of the Taiwan fold-and-thrust belt, given the observed fluid pressures and decollement dip. No extraordinary rock properties, such as extremely elevated fluid pressures or extremely weak basal layers, need to be called on to explain the process of mountain building in Taiwan or, by implication, elsewhere.

To assess the sensitivity of this conclusion to our use of Byerlee's law on the base, we show in Figure 15 a plot of μ versus μ_b consistent with $\alpha = 2.9^\circ$ and $\beta = 6^\circ$ for three fluid pressure ratios $\lambda = 0.4, 0.7$, and 0.85 . Values as low as $\mu = \mu_b = 0.2$ or as high as $\mu = \mu_b = 1.75$ can satisfy the Taiwan data. In general, for any basal friction permitted by uncertainties in the laboratory results, say $0.6 \leq \mu_b \leq 0.9$, the corresponding value of the effective internal friction μ must be about 20% larger. If $\mu_b = 0.85$, the shear traction on the basal decollement at a depth $H = 10$ km is $\tau_b = 65$ MPa, assuming $\rho = 2.4$ g/cm³. This can be reduced to as low as $\tau_b = 15$ MPa if $\mu_b = 0.2$, which cannot be ruled out by our data.

It should also be remarked that the inferred excess of effective internal friction over basal friction depends rather critically on the assumption that $\lambda = \lambda_b$. In fact, a solution having $\mu = \mu_b = 0.85$ with λ_b only 10% greater than $\lambda = 0.675$ is also consistent with the observed wedge geometry α

$= 2.9^\circ$ and $\beta = 6^\circ$. The essential requirement is that the interior of the wedge be slightly stronger than the base, for whatever reason. Since there is no evidence in any of the well data for even marginally greater overpressures on or below the decollement, we are led to conclude that $\mu > \mu_b$.

APPLICATIONS TO OTHER AREAS

In other areas of active plate compression we have fewer constraints on decollement dip and fluid pressure gradient than in Taiwan. However, some information on decollement dip is now available through seismic reflection profiling or refraction studies in a number of active submarine accretionary wedges (for example, Beck and Lehner [1974], Seely et al. [1974], and others). Therefore by assuming the same values of rock strength and friction as we found in Taiwan, namely, $\mu_b = 0.85$ and $\mu = 1.03$, we may compute a predicted fluid pressure coefficient $\lambda = \lambda_b$ given the observed taper of the wedge (Figure 16 and Table 1). By assuming that $\lambda = \lambda_b$ instead of allowing for the possibility in some wedges that $\lambda < \lambda_b$, we may upwardly bias our predicted value of the fluid pressure ratio within the wedge and downwardly bias our prediction on the basal decollement; usually only the former, if either, is constrained by drilling. Note in addition that our indirect fluid pressure determination is least susceptible to errors in α or β for large values of $\lambda = \lambda_b$; this is apparent in Figure 17, which shows α versus β for various fluid pressure ratios.

The well-known [Beck and Lehner, 1974; Hamilton, 1979] seismic profile across the Java Trench south of Bali predicts $\lambda = 0.7$. A profile of the Makran wedge in the Gulf of Oman

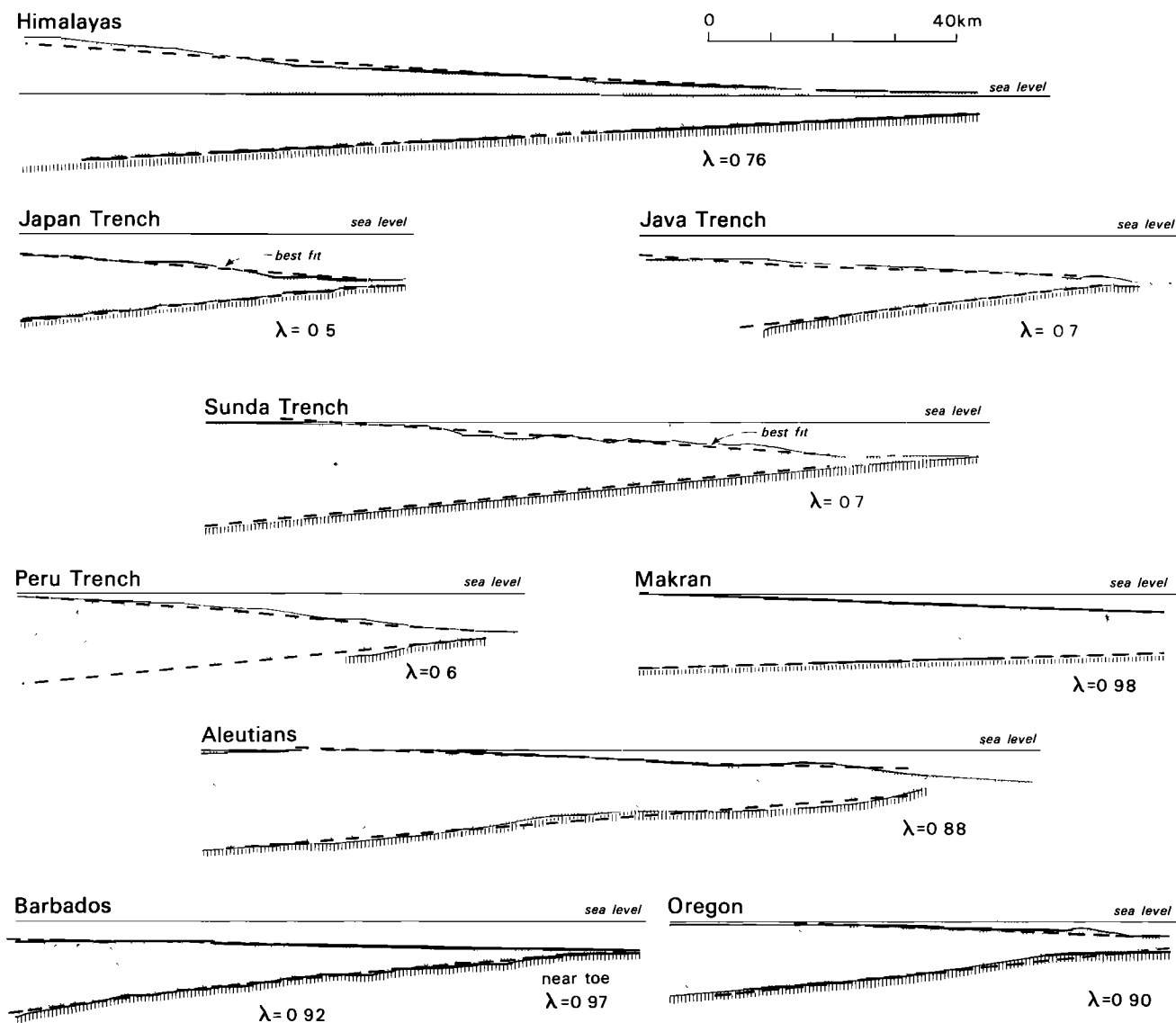


Fig. 16. Cross sections of the Himalayan fold-and-thrust belt and various active submarine accretionary wedges. Heavy dashed lines are best fitting linear profiles used to infer the fluid pressure ratios $\lambda = \lambda_b$, which are also shown.

[White and Ross, 1979] just offshore from mud volcanoes and near a well showing extreme overpressures (J. Harms, private communication, 1982) predicts $\lambda = 0.98$. The International Program of Ocean Drilling (IPOD) transect of the Japan Trench [Nasu et al., 1979] predicts $\lambda = 0.5$. Gravity modeling of the Sunda Arc [Kieckhefer et al., 1981] and seismic reflection modeling of the Peru Trench [Keller et al., 1979] yield tapers corresponding, respectively, to $\lambda = 0.7$ and $\lambda = 0.6$. The eastern Aleutians section of von Huene et al. [1979] in the Gulf of Alaska predicts $\lambda = 0.88$; a similar maximum fluid pressure ratio of $\lambda = 0.87$ was reported by Hottman et al. [1979] for nearby wells in shallow water to the north. The Oregon section of Snavely et al. [1980] predicts $\lambda = 0.9$, in good agreement with fragmentary well data on the shelf indicating $\lambda = 0.85$ [Moore and von Heune, 1980]. Using values of decollement dip from Seeber et al. [1981] and topographic slopes from Ohta and Akiba [1973], we calculate $\lambda = 0.76$ for the Himalaya. The Middle America Trench off Guatemala and southern Mexico has a taper [Seely et al., 1974; Moore et al., 1979] that predicts $\lambda = 0.7$,

which is consistent with the strong indirect evidence of high overpressures observed qualitatively at several sites within the wedge during drilling operations conducted on Deep Sea Drilling Project (DSDP) leg 84 [Aubouin et al., 1982]. The wedge of the Lesser Antilles extending east from Barbados has an overall taper [Westbrook, 1975] corresponding to a predicted fluid pressure ratio $\lambda = 0.92$. Measured ratios λ reach 0.8 in deeper wells in Barbados, in adequate agreement with this prediction. Near the toe the taper narrows perceptibly [Moore et al., 1982], indicating an even greater fluid pressure ratio, namely, $\lambda > 0.97$. This was confirmed by direct measurements indicating $\lambda \approx 1$ at the bottom of DSDP hole 542 (leg 78A), which is located only $1\frac{1}{2}$ km inward from the deformation front. This is the only near-toe direct fluid pressure measurement available in any accretionary wedge.

In summary, the predicted fluid pressure coefficients λ for various accretionary wedges of known taper are all in excess of hydrostatic ($\lambda \geq 0.4$), which is reasonable in light of pressures normally encountered in deep drilling [Fertl,

TABLE 1. Geometries of Active Fold-and-Thrust Belts and Accretionary Wedges and the Corresponding Inferred Fluid Pressure Ratios $\lambda = \lambda_b$, Compared With Available Direct Fluid Pressure Measurements—Qualitative Bounds on the Inferred Values of $\lambda = \lambda_b$ Due to Uncertainties in α and β Can Be Gaged From Figure 17

	α , deg	β , deg	$\alpha + \beta$ Source	Predicted $\lambda = \lambda_b$	Observed λ	λ Source
<i>Subaerial</i>						
Taiwan	2.9 ± 0.3	6.0 ± 0.5	This paper, <i>Suppe</i> [1980b, 1981]	...	0.675 ± 0.05	extensive well measurements; <i>Suppe and Wittke</i> [1977], unpublished data
Himalaya	4.0 ± 0.5	3.0 ± 1.0	<i>Ohta and Akiba</i> [1973], <i>Seeber et al.</i> [1981]	0.76
<i>Submarine</i>						
Japan	4.5 ± 0.5	5.4 ± 0.5	<i>Nasu et al.</i> [1979]	0.5
Peru	3.8 ± 0.3	5.9 ± 1.0	<i>Keller et al.</i> [1979]	0.6
Java	3.1 ± 0.3	6.6 ± 1.0	<i>Hamilton</i> [1979]	0.7
Sunda	4.0 ± 1.0	5.0 ± 1.0	<i>Kieckhefer et al.</i> [1981]	0.7
Guatemala	5.7 ± 0.7	2.5 ± 1.0	<i>Seeley et al.</i> [1974]	0.7	high	indirect evidence; DSDP Leg 84 drilling; <i>Aubouin et al.</i> [1982]
Aleutians	3.0 ± 0.5	4.5 ± 1.0	<i>von Huene et al.</i> [1979]	0.88	~ 0.87	mud weight in a well in ponded sediments; <i>Hottman et al.</i> [1979]
Oregon	2.1 ± 0.5	6.0 ± 1.0	<i>Snavely et al.</i> [1980]	0.90	0.85 ± 0.03	mud weight in a well on the shelf; <i>Moore and von Huene</i> [1980]
Barbados	1.0 ± 0.5	8.0 ± 0.8	<i>Westbrook</i> [1975]	0.92	0.8 ± 0.05	mud weight in a well on Barbados; <i>Moore and von Huene</i> [1980]
Overall taper						
Near toe	0.7 ± 0.2	4.5 ± 0.5	<i>Moore et al.</i> [1982]	0.97	~ 1	inadvertent packer experiment in hole 542; <i>Moore et al.</i> [1982]
Makran	1.6 ± 0.3	2.0 ± 1.0	<i>White and Ross</i> [1979]	0.98	~ 1	mud weight in a well offshore Pakistan; Harms (private communication, 1982)

1976]. In addition, the values found in eastern Aleutians, Oregon, Guatemala, Makran, and Barbados are in good agreement with fragmentary nearby well data. Furthermore, no tapers are observed that lie outside the range predicted by the theory (Figure 17). These observations further support our Coulomb wedge analysis as a valid first-order theory.

EFFECTS OF ISOSTASY AND EROSION ON TAPER

Isostatic adjustment in response to the overburden that is added by growth of the wedge can result in some degree of reinitiation of deformation within the wedge. The greater stacking of thrust sheets toward the back of the wedge will

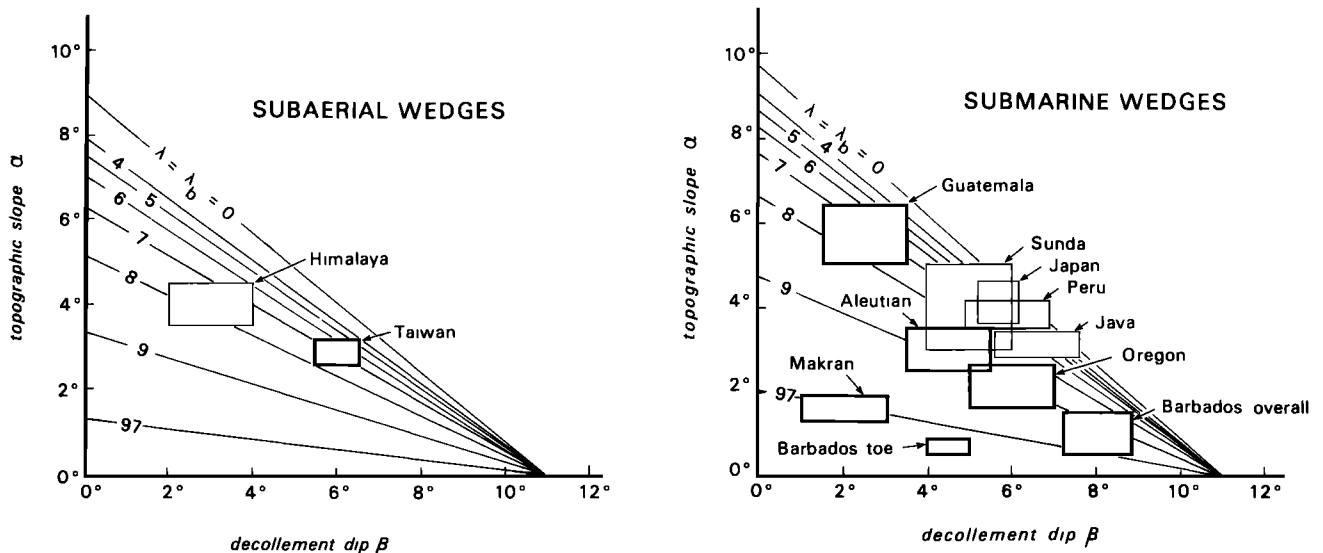


Fig. 17. Theoretical linear relationships $\alpha + R\beta = F$ for various fluid pressure ratios $\lambda = \lambda_b$, assuming $\mu_b = 0.85$ and $\mu = 1.03$. Boxes indicate observed geometries of active wedges, used to infer the fluid pressure ratios within them. Heavy outlines indicate those wedges for which some direct fluid pressure information is available. A rock density $\rho = 2.4 \text{ g/cm}^3$ was used in the submarine case; other values would yield very similar results as the sensitivity to ρ is slight.

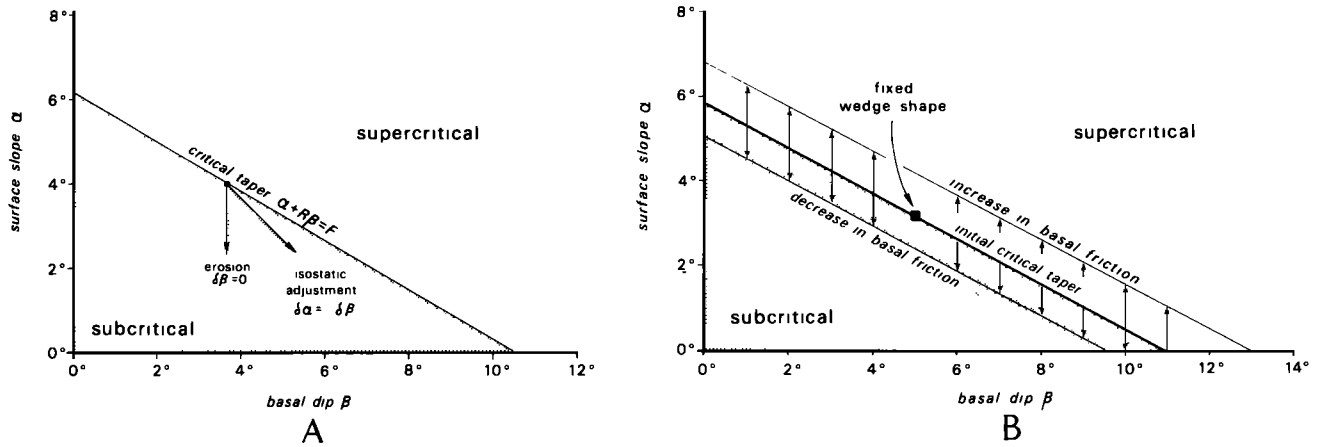


Fig. 18. Diagram illustrating the effects on wedge geometry of (a) surficial erosion or isostatic adjustment and (b) a change in basal friction, either in λ_b or μ_b . Both erosion and isostatic adjustment drive a critical wedge into the subcritical regime, encouraging renewed deformation. An increase in basal friction which does not violate the condition $(1 - \lambda_b)\mu_b \leq (1 - \lambda)\mu$ also encourages deformation, to produce a steeper critically tapered wedge. A decrease in basal friction, on the other hand, gives rise to a supercritical wedge and possibly to subduction unaccompanied by accretion or wedge deformation. The sensitivity to changes in basal friction is quite pronounced. The hypothetical case depicted here represents only a $\pm 2\%$ change in λ_b of a submarine wedge having $\lambda = \lambda_b = 0.8$ initially.

tend to result in a greater degree of downward isostatic adjustment there than in the front. This results in an increase $\delta\beta$ in the dip of the basal decollement. Because total wedge taper is conserved in the isostatic process, i.e., $\delta\alpha + \delta\beta = 0$, the topographic slope α is correspondingly reduced.

The critical taper equation (19) shows that the criticality of a wedge depends on how its taper is partitioned between topographic slope α and basement dip β . Because the coefficient R given by (20) is always less than 1 for reasonable densities ρ and ρ_w , each degree of α in the wedge taper is less effective in attaining critical taper than is a degree of β . Therefore the exchange of α for β during isostatic adjustment causes the wedge to become subcritical and encourages renewed deformation within the wedge until a new critical taper is attained (Figure 18a).

Erosion also acts to induce deformation within the wedge by reducing the topographic slope while leaving the decollement dip unaltered, thus producing a subcritical taper (Figure 18a). In an active fold-and-thrust belt, the processes of erosion and internal deformation should be constantly occurring at rates sufficient to counteract each other, as they are in western Taiwan. Sudden climatic increases in erosive flux or tectonic decreases in compressive flux will cause disequilibrium wedge shapes [Suppe, 1981].

Erosion at the upper wedge surface is not likely to be important in a submerged accretionary wedge. Accretion at the front of the wedge should in that case be the major source of continued wedge deformation. The addition of extra mass at the front of an already critical wedge results in a taper-preserving series of deformations, which enlarge the wedge by propagating toward the back. Sedimentation on top of the wedge may make it supercritical. For these reasons, as well as those enumerated below, the kinematics of subaerial and submarine wedges should be substantially different.

EFFECTS OF FLUCTUATIONS IN BASAL FRICTION

In the preceding discussion we have ignored possible time variations in the physical properties of either the wedge (μ and λ) or the decollement (μ_b and λ_b). Time variation in basal

shear traction is most likely in long-lived, slowly accreting submarine wedges where the rate of subduction of the underlying oceanic plate is fast. It is less likely in steady state subaerial wedges like Taiwan where, because of the thick stratigraphic section and the high erosive fluxes, most of the accreted material remains in the wedge for at most a few million years prior to erosion.

Consider a submarine wedge initially at critical taper. If this wedge experiences a drop in basal friction, perhaps by encountering a stratigraphic change in decollement material, the critical taper will decrease and the previously critical wedge now will be at supercritical taper (Figure 18b). In contrast, if the wedge experiences a modest increase in basal friction, the critical taper will increase and the now subcritical wedge will deform until the new critical taper is attained (Figure 18b). If the new basal material has properties such that $(1 - \lambda_b)\mu_b > (1 - \lambda)\mu$, it cannot form a decollement and a new decollement must form higher within the existing wedge. Under these conditions the wedge undergoes tectonic erosion along its base.

We might expect, from the above considerations, to find some submarine wedges that are at supercritical taper, recording a past period of higher basal friction. If a wedge is currently supercritical, the fluid pressure ratio $\lambda = \lambda_b$ we infer from its taper will be an underestimate. Oceanic sediments can be subducted beneath a supercritical wedge without offscraping and accretion. We might also expect, from the above considerations, to find some submarine wedges that are undergoing subduction-erosion or loss of material from their base because of a recent increase in basal friction beyond $(1 - \lambda_b)\mu_b = (1 - \lambda)\mu$. Nonaccreting and negatively accreting wedges are being increasingly recognized [for example, von Huene et al., 1980; Aubouin et al., 1982].

REALM OF THE THEORY

A further method of testing the validity of the Coulomb wedge theory is to examine natural cases in which the theory would be expected to break down in some expected way. Two situations will be considered: (1) the basal decollement

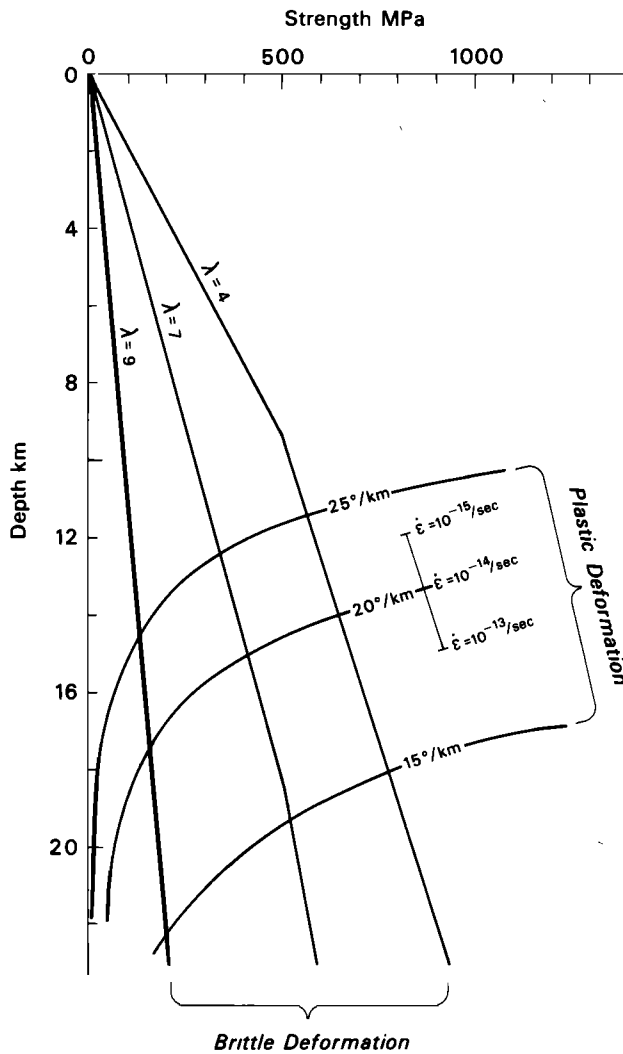


Fig. 19. Rock strength, as measured by the stress difference $\sigma_1 - \sigma_3$, versus depth in the earth, assuming frictional behavior $|\tau| = 0.85\sigma_n^*$ for $\sigma_n^* < 200$ MPa and $|\tau| = 50$ MPa + $0.6\sigma_n^*$ for $\sigma_n^* > 200$ MPa [Byerlee, 1978] for the near-surface brittle deformation and quartz plastic flow governed by $\dot{\epsilon} = 5 \times 10^{-6} (\sigma_1 - \sigma_3)^3 \exp(-0.19 \text{ MJ mol}^{-1}/RT)$, where $\dot{\epsilon}$ is in s^{-1} and $\sigma_1 - \sigma_3$ is in MPa [Brace and Kohlstedt, 1980] at depth. The plastic strength has been calculated for a range of geothermal gradients and geologically reasonable strain rates. The theoretical strength is greatest at the point of brittle-plastic transition, where the brittle and plastic strengths are equal.

exhibits pressure-independent plastic rather than Coulomb behavior because of rock type, and (2) the thickness of the wedge exceeds the depth to the brittle-plastic transition so that the base no longer displays Coulomb friction because of high temperature. In either case we may deduce the expected qualitative behavior by rewriting the critical taper equation (18) directly in terms of the basal shear traction (8), i.e.,

$$\alpha + \beta = \frac{\tau_b/\rho g H + (1 - \rho_w/\rho)\beta}{(1 - \rho_w/\rho) + (1 - \lambda)K} \quad (33)$$

If τ_b is limited by a yield stress that does not depend on pressure, the ratio $\tau_b/\rho g H$ and thus the surface slope α should decrease toward the back of the wedge where the thickness H is greater. If the yield stress is low so that $\tau_b \ll \rho g H$, the coefficient K in the denominator of (33) can be adequately approximated by $K \approx 2 \sin \phi / (1 - \sin \phi)$.

The principal situation in which a relatively thin, low-temperature wedge might be expected to exhibit basal plasticity is a decollement composed of evaporites, as observed in some ancient fold-and-thrust belts. A well-known active fold-and-thrust belt with a low-strength salt decollement occurs in the Zagros Mountains [Stocklin, 1968]; here even away from the toe we observe an abnormally small surface slope and taper relative to the typical Coulomb wedge prediction, as we expect. Similarly, the Salt Range of Pakistan has an abnormally low surface slope.

As an accretionary wedge or fold-and-thrust belt grows, its basal decollement may become sufficiently deep that the assumption of brittle behavior is no longer valid because thermally activated deformation processes prevail. The depth of the brittle-plastic transition for quartz [Brace and Kohlstedt, 1980] and feldspar (W. F. Brace, private communication, 1982) is expected to occur at a depth of roughly 12 to 16 km in regions with moderate geothermal gradients (Figure 19). Below such depths, sliding resistance along the basal decollement drops rapidly and is independent of pressure. The Taiwan wedge is too small to reach the depth of brittle-plastic transition, so Coulomb wedge theory is applicable throughout. However, the Coulomb theory is not expected to be valid toward the interior of very wide mountain ranges and accretionary wedges. They frequently show an abrupt drop in surface slope toward their interior, which is interpreted as the surface expression of the brittle-plastic transition along the base (for example, see Figure 20). The same phenomenon provides a natural explanation for the break in topographic slope in the Higher Himalaya near the edge of the Tibetan Plateau and for the edge of the Altiplano of the Andes.

CONCLUSIONS

The idea that fold-and-thrust belts and accretionary wedges have the mechanics of bulldozer wedges at failure in horizontal compression has been verified quantitatively in this paper. An approximate theory has been derived for the minimum or critical taper required for a Coulomb wedge to slide stably along its basal decollement rather than deform internally. If the basal friction increases, so does the taper, whereas an increase in the internal strength of the wedge decreases the critical taper. The observed tapers of active accretionary wedges are consistent with low apparent cohesive strengths and with coefficients of basal sliding friction

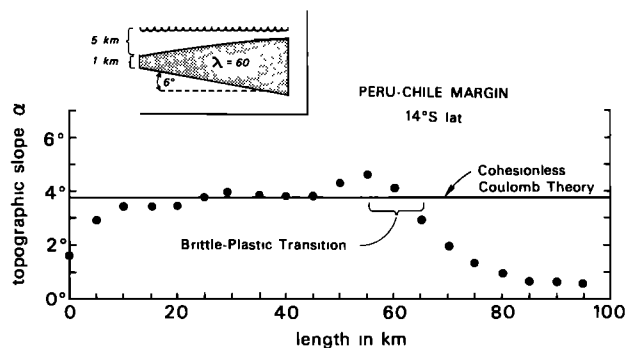


Fig. 20. Surface slope of Peruvian continental margin along latitude 14°S as a function of distance from trench. The decrease in surface slope beyond 55 km is interpreted to reflect a reduced basal resistance, where the base of the wedge extends below the brittle-plastic transition.

$\mu_b = 0.85$ and apparent internal friction $\mu = 1.03$. The roughly 20% difference between μ_b and μ required to fit the observed taper of the fold-and-thrust belt in western Taiwan is interpreted in terms of the two aspects of deformation within the wedge. First, the preexisting fractures are sufficient only to allow frictional sliding on a limited number of generally suboptimally oriented surfaces, and second, it is frequently necessary to fracture locked geological structures for continued deformation.

Two important differences exist between subaerial and submarine wedges.

1. The horizontal gradient in buoyancy caused by the sloping rock-water interface gives rise to a term involving ρ_w/ρ in the critical taper equation (22). This term disappears discontinuously as the wedge emerges above sea level and should produce about a 1° drop in surface slope; such a drop, although somewhat larger, is observed in eastern Taiwan (see Figure 10).

2. Erosion requires continued deformation throughout a subaerial wedge to maintain the critical surface slope over the length of the wedge. In contrast, submarine wedges deform mostly in the toe where new material is encountered and they may be supercritical away from the toe because of sedimentation and fluctuations in basal friction. Observed instances of subduction without accretion or subduction-erosion in some submarine wedges may also be effects of fluctuation in basal friction.

The critical taper of fold-and-thrust belts and accretionary wedges is sensitive to the pore fluid pressure ratio λ , particularly so for values of λ near 1. The Coulomb wedge theory is tested by computing λ for a number of active accretionary wedges and fold-and-thrust belts based on their observed tapers. Fluid overpressures ($\lambda \approx 0.4$) are predicted in every case, and the computed values of λ are in good agreement with fragmentary nearby well data where they exist.

The Coulomb theory is expected to break down where the wedge thickens to the depth of the brittle-plastic transition, below which the basal resistance to sliding should drop abruptly with increasing temperature. Both the Andean and Himalayan wedges display this predicted drop in taper where they reach a thickness of about 15 km, which agrees well with the depth of the brittle-plastic transition in quartz for typical geothermal gradients.

We conclude that fold-and-thrust belts and accretionary wedges have the overall mechanics of a bulldozer wedge at failure in horizontal compression and that normal laboratory fracture and frictional strengths are appropriate to mountain-building processes in the upper crust, above the brittle-plastic transition.

Acknowledgments. We are pleased to acknowledge Florian Lehner and Leonie Davis for their help in early stages of this work in 1977 and 1978. Brian Evans, Jason Morgan, Sean Solomon, Tom Crough, David Elliott, and an anonymous reviewer offered many useful suggestions for which we are grateful. Dave Smith measured the surface slopes offshore of Peru (Figure 20). J. Suppe would like to thank the Chinese Petroleum Corporation for access to data and hospitality in Taiwan and the John Simon Guggenheim Memorial Foundation for gracious and unencumbered support in 1978–1979. This work was supported by the Division of Earth Sciences, National Science Foundation, grants EAR80-18350 and EAR81-21197 at Princeton and grant EAR78-12936 at MIT.

This paper is dedicated to W. M. Chapple, who died in February 1981. Our work was stimulated by a lecture he gave at Princeton in 1977.

REFERENCES

- Aubouin, J., R. von Huene, M. Baltuck, R. Arnott, J. Bourgeois, M. Filewicz, K. Kvenvolden, B. Leinert, J. McDonald, K. McDougall, Y. Ogawa, E. Taylor, and B. Winsborough, Leg 84 of the Deep Sea Drilling Project, subduction without accretion: Middle America Trench off Guatemala, *Nature*, 297, 458–460, 1982.
- Bally, A. W., P. L. Gordy, and G. A. Stewart, Structure, seismic data and orogenic evolution of southern Canadian Rocky Mountains, *Bull. Can. Pet. Geol.*, 14, 337–381, 1966.
- Beck, R. H., and P. Lehner, Oceans, new frontier in exploration, *Am. Assoc. Pet. Geol. Bull.*, 58, 376–395, 1974.
- Brace, W. F., and D. L. Kohlstedt, Limits on lithospheric stress imposed by laboratory experiments, *J. Geophys. Res.*, 85, 6248–6252, 1980.
- Byerlee, J., Friction of rocks, *Pure Appl. Geophys.*, 116, 615–626, 1978.
- Chapple, W. M., Mechanics of thin-skinned fold-and-thrust belts, *Geol. Soc. Am. Bull.*, 89, 1189–1198, 1978.
- Chi, W. R., J. Namson, and J. Suppe, Stratigraphic record of plate interactions in the Coastal Range of eastern Taiwan, *Geol. Soc. China Mem.*, 4, 491–530, 1981.
- Davis, D. M., The mechanics of thrust faults: A sand box model, B.S. thesis, 53 pp., Princeton Univ., Princeton, N.J., 1978.
- Davis, D. M., and J. Suppe, Critical taper in mechanics of fold-and-thrust belts, *Geol. Soc. Am. Abstr. Programs*, 12, 410, 1980.
- Elliott, D., The motion of thrust sheets, *J. Geophys. Res.*, 81, 949–963, 1976.
- Goldburg, B. L., Formation of critical taper wedges by compression in a sand box model, B.S. thesis, 70 pp., Princeton Univ., Princeton, N.J., 1982.
- Hamilton, W., Tectonics of the Indonesian region, *U.S. Geol. Surv. Prof. Pap.*, 1078, 345 pp., 1979.
- Hoshino, K., H. Koide, K. Inami, S. Iwamura, and S. Mitsui, Mechanical properties of Japanese Tertiary sedimentary rocks under high confining pressures, *Rep.* 244, 200 pp., Geol. Surv. of Japan, Kawasaki, 1972.
- Hottman, C. E., J. H. Smith, and W. R. Purcell, Relationship among earth stresses, pore pressure, and drilling problems offshore Gulf of Alaska, *J. Pet. Technol.*, 31, 1477–1484, 1979.
- Hubbert, M. K., and W. W. Rubey, Role of fluid pressure in mechanics of overthrust faulting, I, Mechanics of fluid-filled solids and its application to overthrust faulting, *Geol. Soc. Am. Bull.*, 70, 115–166, 1959.
- Jaeger, J. C., and N. G. W. Cook, *Fundamentals of Rock Mechanics*, pp. 87–91, Methuen, London, 1969.
- Keller, B., B. T. R. Lewis, C. Meeder, C. Helsley, and R. P. Meyer, Explosion seismology studies of active and passive continental margins, in *Geological and Geophysical Investigations of Continental Margins*, Mem. 29, edited by J. S. Watkins, L. Montadert, and P. Dickerson, pp. 443–451, American Association of Petroleum Geologists, Tulsa, Okla., 1979.
- Kieckhefer, R. M., G. F. Moore, F. J. Emmel, and W. Sugiarta, Crustal structure of the Sunda forearc region west of central Sumatra from gravity data, *J. Geophys. Res.*, 86, 7003–7012, 1981.
- Lambe, T. W., and R. V. Whitman, *Soil Mechanics*, SI version, p. 69, John Wiley, New York, 1979.
- Li, Y. H., Denudation of Taiwan island since the Pliocene epoch, *Geology*, 4, 105–107, 1976.
- McClay, K. R., and N. J. Price (Eds.), *Thrust and Nappe Tectonics*, Spec. Publ. 9, 539 pp., Geological Society of London, Oxford, 1981.
- Moore, J. C., and R. von Huene, Abnormal pore pressure and hole instability in forearc regions: A preliminary report, report, 29 pp., Ocean Margin Drill. Proj., Menlo Park, Calif., 1980.
- Moore, J. C., J. S. Watkins, T. H. Shipley, S. B. Bachman, F. W. Beghtel, A. Butt, B. M. Didyk, J. K. Leggett, N. Lundberg, K. J. McMillen, N. Niitsuma, L. E. Shephard, J.-F. Stephan, and H. Stradner, Progressive accretion in the Middle America Trench, southern Mexico, *Nature*, 281, 638–642, 1979.
- Moore, J. C., et al., Offscraping and underthrusting of sediment at the deformation front of the Barbados Ridge: Deep Sea Drilling Project leg 78A, *Geol. Soc. Am. Bull.*, 93, 1065–1077, 1982.
- Namson, J. S., Studies of the structure, stratigraphic record of plate interaction and role of pore-fluid pressure in the active fold and thrust belt of Taiwan and a study of manganese deposits from

- northern California, Ph.D. thesis, 302 pp., Princeton Univ., Princeton, N.J., 1982.
- Nasu, N., Y. Tomoda, K. Kobayashi, H. Kagami, S. Uyeda, S. Nagumo, I. Kushiro, M. Ozima, K. Nakazawa, Y. Takayanagi, H. Okada, S. Murauchi, Y. Ishiwada, and Y. Ishii, Multi-channel seismic reflection data across the Japan Trench, *IPOD-Japan Basic Data Ser.*, No. 3, 22 pp., Ocean Res. Inst., Univ. of Tokyo, Tokyo, 1979.
- Ohta, Y., and C. Akiba (Eds.), *Geology of the Nepal Himalayas*, 286 pp., Himalayan Committee of Hokkaido University, Saporro, Japan, 1973.
- Paterson, M. S., *Experimental Rock Deformation: The Brittle Field*, pp. 16–50, Springer-Verlag, New York, 1978.
- Roeder, D., O. E. Gilbert, Jr., and W. D. Witherspoon, Evolution and macroscopic structure of Valley and Ridge thrust belt, Tennessee and Virginia, *Stud. in Geol.* 2, 25 pp., Dep. of Geol. Sci., Univ. of Tenn., Chattanooga, 1978.
- Seeber, L., J. G. Armbruster, and R. C. Quittmeyer, Seismicity and continental subduction in the Himalayan arc, in *Zagros-Hindu Kush-Himalaya Geodynamic Evolution, Geodynamics Ser.*, vol. 3, edited by H. K. Gupta, and F. M. Delany, pp. 215–242, AGU, Washington, D.C., 1981.
- Seely, D. R., P. R. Vail, and G. G. Walton, Trench slope model, in *The Geology of Continental Margins*, edited by C. A. Burk, and C. L. Drake, pp. 249–260, Springer-Verlag, New York, 1974.
- Seno, T., The instantaneous rotation vector of the Philippine Sea plate relative to the Eurasian plate, *Tectonophysics*, 42, 209–226, 1977.
- Snively, P. D., Jr., H. C. Wagner, and D. L. Lander, Geologic cross section of the central Oregon continental margin, *Geol. Soc. Am. Map Chart Ser.*, MC-28J, 1980.
- Stanley, R. S., L. B. Hill, H. C. Chang, and H. N. Hu, A transect through the metamorphic core of the Central Mountains, southern Taiwan, *Geol. Soc. China Mem.*, 4, 443–473, 1981.
- Stocklin, J., Structural history and tectonics of Iran: A review, *Am. Assoc. Pet. Geol. Bull.*, 52, 1229–1258, 1968.
- Stockmal, G. S., and W. M. Chapple, Modelling accretionary wedge deformation using a rigid-perfectly plastic rheology (abstract), *Eos Trans. AGU*, 62, 397–398, 1981.
- Suppe, J., A retrodeformable cross section of northern Taiwan, *Geol. Soc. China Proc.*, 23, 46–55, 1980a.
- Suppe, J., Imbricated structure of western foothills belt, south-central Taiwan, *Pet. Geol. Taiwan*, 17, 1–16, 1980b.
- Suppe, J., Mechanics of mountain building and metamorphism in Taiwan, *Geol. Soc. China Mem.*, 4, 67–89, 1981.
- Suppe, J., and J. Namson, Fault-bend origin of frontal folds of the western Taiwan fold-and-thrust belt, *Pet. Geol. Taiwan*, 16, 1–18, 1979.
- Suppe, J., and J. H. Wittke, Abnormal pore-fluid pressures in relation to stratigraphy and structure in the active fold-and-thrust belt of northwestern Taiwan, *Pet. Geol. Taiwan*, 14, 11–24, 1977.
- Suppe, J., J. Namson, and A. M. Pytte, Role of fluid pressure in an active overthrust belt: Taiwan, *Geol. Soc. Am. Abstr. Programs*, 13, 562, 1981.
- Tsai, Y. B., T. L. Teng, J. M. Chiu, and H. L. Liu, Tectonic implications of the seismicity of the Taiwan region, *Geol. Soc. China Mem.*, 2, 13–41, 1977.
- von Huene, R., G. W. Moore, and J. C. Moore, Cross section of Alaska Peninsula-Kodiak Island-Aleutian Trench, *Geol. Soc. Am. Map Chart Ser.*, MC-28A, 1979.
- von Huene, R., M. Langseth, N. Nasu, and H. Okada, Summary, Japan Trench Transect, *Initial Rep. Deep Sea Drill. Proj., Legs 56 and 57*, 473–488, 1980.
- Westbrook, G. K., The structure of the crust and upper mantle in the region of Barbados and the Lesser Antilles, *Geophys. J. R. Astron. Soc.*, 48, 201–242, 1975.
- White, R. S., and D. A. Ross, Tectonics of the western Gulf of Oman, *J. Geophys. Res.*, 84, 3479–3489, 1979.
- Wu, F. T., Recent tectonics of Taiwan, in *Geodynamics of the Western Pacific, Adv. in Earth and Planet. Sci.* 6, edited by S. Uyeda, R. W. Murphy, and K. Kobayashi, pp. 265–299, Center for Academic Publications Japan, Tokyo, 1979.
- Wu, F. T., Y. H. Yeh, and Y. B. Tsai, Seismicity in the Tsengwen reservoir area, Taiwan, *Bull. Seismol. Soc. Am.*, 69, 1783–1796, 1979.

(Received January 25, 1982;
revised August 24, 1982;
accepted November 5, 1982.)